Global Biogeochemical Cycles

RESEARCH ARTICLE
10.1029/2024GB008156

Special Collection:
Regional Carbon Cycle Assessment and Processes - 2

Observational and Numerical Modeling Constraints on the Global Ocean Biological Carbon Pump

Scott C. Doney[1], Kayla A. Mitchell[1,2], Stephanie A. Henson[3], Emma Cavan[4], Tim DeVries[5], Nicolas Gruber[6], Judith Hauck[7], Colleen B. Mouw[8], Jens D. Müller[6], and Francois W. Primeau[2]

[1]Department of Environmental Sciences, University of Virginia, Charlottesville, VA, USA, [2]Department of Earth System Science, University of California, Irvine, Irvine, CA, USA, [3]National Oceanography Centre, Southampton, UK, [4]Department of Life Sciences, Silwood Park Campus, Imperial College London, Berkshire, UK, [5]Department of Geography, Earth Research Institute, University of California, Santa Barbara, Santa Barbara, CA, USA, [6]Environmental Physics, Institute of Biogeochemistry and Pollutant Dynamics, ETH Zurich, Zürich, Switzerland, [7]Alfred-Wegener-Institut, Helmholtz-Zentrum für Polar- und Meeresforschung, Bremerhaven, Germany, [8]Graduate School of Oceanography, University of Rhode Island, Narragansett, RI, USA

Abstract This study characterized ocean biological carbon pump metrics in the second iteration of the REgional Carbon Cycle Assessment and Processes (RECCAP2) project. The analysis here focused on comparisons of global and biome-scale regional patterns in particulate organic carbon (POC) production and sinking flux from the RECCAP2 ocean biogeochemical model ensemble against observational products derived from satellite remote sensing, sediment traps, and geochemical methods. There was generally good model-data agreement in mean large-scale spatial patterns, but with substantial spread across the model ensemble and observational products. The global-integrated, model ensemble-mean export production, taken as the sinking POC flux at 100 m (6.08 ± 1.17 Pg C yr^{-1}), and export ratio defined as sinking flux divided by net primary production (0.154 ± 0.026) both fell at the lower end of observational estimates. Comparison with observational constraints also suggested that the model ensemble may have underestimated regional biological CO_2 drawdown and air-sea CO_2 flux in high productivity regions. Reasonable model-data agreement was found for global-integrated, ensemble-mean sinking POC flux into the deep ocean at 1,000 m (0.65 ± 0.24 Pg C yr^{-1}) and the transfer efficiency defined as flux at 1,000 m divided by flux at 100 m (0.122 ± 0.041), with both variables exhibiting considerable regional variability. The RECCAP2 analysis presents standard ocean biological carbon pump metrics for assessing biogeochemical model skill, metrics that are crucial for further modeling efforts to resolve remaining uncertainties involving system-level interactions between ocean physics and biogeochemistry.

Plain Language Summary Phytoplankton in the surface ocean create each year an amount of organic carbon approximately equivalent to all the annual photosynthesis by plants on land. A small fraction of this newly formed organic carbon is exported below the surface layer, and an even smaller amount makes it all the way to the deep ocean. The transport of organic carbon to the sub-surface ocean, called the biological carbon pump, influences the global-scale distributions of ocean nutrients, oxygen, and inorganic carbon as well as the amount of carbon dioxide in the atmosphere. The global rates and geographic patterns of photosynthesis and carbon flux out of the surface ocean have previously been constructed from ship measurements and satellite remote sensing. Here, we compare these observation-based estimates to a suite of three-dimensional numerical ocean models and find broadly similar results. The model simulations also capture aspects of the biological carbon pump deeper in the water column, where there are fewer direct constraints from field observations. Our comparison of observations and simulations identifies some deficiencies in the models that should be corrected in order to better simulate climate change impacts on the biological carbon pump.

Key Points:

- Global-scale, ocean biogeochemical simulations are compared with observation-based estimates of the marine biological carbon pump
- A multi-model ensemble exhibits good agreement with observation-based metrics for carbon export flux and transfer efficiency
- Based on identified model-observation and inter-model differences, we provide guidance for future model evaluations and development

Supporting Information:

Supporting Information may be found in the online version of this article.

Correspondence to:

S. C. Doney,
sdoney@virginia.edu

Citation:

Doney, S. C., Mitchell, K. A., Henson, S. A., Cavan, E., DeVries, T., Gruber, N., et al. (2024). Observational and numerical modeling constraints on the global ocean biological carbon pump. *Global Biogeochemical Cycles*, *38*, e2024GB008156. https://doi.org/10.1029/2024GB008156

Received 4 MAR 2024
Accepted 17 JUN 2024

Author Contributions:

Conceptualization: Scott C. Doney, Stephanie A. Henson
Data curation: Kayla A. Mitchell, Jens D. Müller
Formal analysis: Scott C. Doney, Kayla A. Mitchell, Stephanie A. Henson
Funding acquisition: Scott C. Doney, Stephanie A. Henson
Investigation: Scott C. Doney, Kayla A. Mitchell, Stephanie A. Henson,

1. Introduction

Marine biogeochemical processes play a central role in the global Earth System, modulating the distribution of inorganic carbon, oxygen, and nutrients within the ocean and the partitioning of carbon between ocean and atmosphere reservoirs (Broecker & Peng, 1982; DeVries, 2022; Iversen, 2023; Sarmiento & Gruber, 2002; Siegel et al., 2023). Because of the strong oceanic influence on atmospheric CO_2 concentration and thus climate, there is considerable scientific focus on quantifying both the baseline and trends in ocean carbon storage and fluxes

Emma Cavan, Tim DeVries, Nicolas Gruber, Judith Hauck, Colleen B. Mouw, Jens D. Müller, Francois W. Primeau
Methodology: Scott C. Doney, Kayla A. Mitchell, Stephanie A. Henson
Project administration: Scott C. Doney, Stephanie A. Henson, Jens D. Müller
Software: Kayla A. Mitchell, Jens D. Müller
Supervision: Scott C. Doney, Stephanie A. Henson, Jens D. Müller
Visualization: Scott C. Doney, Kayla A. Mitchell
Writing – original draft: Scott C. Doney, Kayla A. Mitchell, Stephanie A. Henson, Emma Cavan
Writing – review & editing: Scott C. Doney, Kayla A. Mitchell, Stephanie A. Henson, Emma Cavan, Tim DeVries, Nicolas Gruber, Judith Hauck, Colleen B. Mouw, Jens D. Müller, Francois W. Primeau

arising from the uptake of anthropogenic CO_2 and climate change impacts on marine biogeochemical and physical dynamics (Canadell et al., 2021; Crisp et al., 2022; DeVries et al., 2019; Gruber et al., 2023; Hauck et al., 2020; Henson et al., 2016; Wilson et al., 2022).

The REgional Carbon Cycle Assessment and Processes (RECCAP) project is a coordinated international effort to constrain contemporary ocean carbon air-sea fluxes and interior storage trends using a combination of observation-based estimates, inverse models, and global ocean biogeochemical models (GOBMs) (Khatiwala et al., 2013; Wanninkhof et al., 2013). The second phase, RECCAP2, extends the original synthesis using additional years of ocean observations and updated methodology and numerical results (DeVries et al., 2023; Hauck et al., 2023) as well as expanding the scope of the analysis, in this case, into biological carbon pump magnitude and efficiency.

In a simple 1-D form, the marine biological carbon pump can be viewed as the net production of particulate organic carbon (POC) and inorganic carbon (PIC) in the surface ocean, downward vertical transport of particulate carbon into the thermocline and deep sea, and subsequent respiration and remineralization of particulate carbon back into dissolved inorganic carbon (DIC) (Volk & Hoffert, 1985). The downward organic carbon transport, or export flux, drives subsurface marine biogeochemistry, fuels deep-ocean ecosystems, and influences ocean carbon storage and atmospheric CO_2. The biological pump accentuates the vertical gradient in DIC already established from CO_2 system thermal solubility and temperature gradients, and deep-ocean carbon storage reflects a net balance between the biological carbon pump source and physical ocean circulation processes that return elevated deep-ocean DIC waters back to the surface ocean via upwelling and vertical mixing (Sarmiento & Gruber, 2006).

The relationship between ocean carbon storage and the strength of the biological pump is not necessarily straightforward because of physical-biological interactions; for example, stronger overturning circulation can enhance both biological export through increased nutrient supply and the physical return of high-DIC deep-ocean waters to the surface (Doney et al., 2006). The vertical structure of the biological carbon pump is also important. Sinking POC fluxes decline rapidly in the thermocline (~100–~1,000 m depth), with only a fraction of surface export flux reaching the deep ocean below 1,000 m (Dinauer et al., 2022; Lima et al., 2014; Lutz et al., 2007; Martin et al., 1987). Deeper remineralization depths, that is the transport of a greater fraction of POC into the lower thermocline or deep ocean prior to respiration, enhance ocean carbon storage because of generally reduced physical return rates to the surface ocean for deeper waters, and therefore longer retention times for the remineralized DIC, although with substantial regional variations associated with circulation pathways and rates (Kwon et al., 2009; Siegel et al., 2021).

Net primary production (NPP) by surface ocean phytoplankton generates POC and dissolved organic carbon (DOC), and most marine NPP is converted rapidly back to DIC through zooplankton grazing of living biomass and detritus or through the microbial loop involving consumption of POC and DOC pools. Export fluxes require an excess of community production of organic carbon over respiration that in turn must be supported by an external supply of new nutrients over sufficient time and space scales (Ducklow & Doney, 2013). The fraction of NPP that is exported (export ratio = export flux/NPP) is modulated by the magnitude and seasonality of NPP, environmental conditions, and phytoplankton and zooplankton community composition (Laufkötter et al., 2016). Export flux from the euphotic zone occurs through multiple pathways including gravitational sinking of POC (e.g., living and dead cells; fecal pellets; marine snow), physical subduction and mixing of POC and DOC below the surface layer, and active biological transport by vertically migrating organisms (Siegel et al., 2016).

Contemporary models capture, with varying levels of sophistication and skill, the biological processes involved in NPP and export flux from the upper ocean (Fennel et al., 2022), though models tend to focus on gravitational particle sinking and many do not incorporate all of the relevant export pathways (Boyd et al., 2019; Henson et al., 2022) or dynamics governing vertical carbon fluxes from the surface to the deep sea (Burd, 2024). Most current GOBMs build from a nutrient-phytoplankton-zooplankton-detritus (NPZD) ecosystem framework (Fennel et al., 2022). Advances from a simple NPZD model include incorporation of multiple dissolved nutrients and micro-nutrients, variable elemental stoichiometry in biomass and detrital pools, plankton functional types spanning size class and taxonomic function, multiple trophic levels, and biomineralization of particulate silicon and calcium carbonate (Hood et al., 2006; Le Quéré et al., 2005; Moore et al., 2004). Phytoplankton growth and NPP rates are governed by nutrient limitation, irradiance, and temperature; growth in some models is also

modulated by variable phytoplankton chlorophyll and cellular nutrient to carbon biomass ratios (Laufkötter et al., 2015).

Models generate particulate detrital material from phytoplankton and zooplankton mortality, grazing, and aggregation; sinking POC, often partitioned into size classes or into free versus mineral associated forms, is a key component of overall export flux (Laufkötter et al., 2016). In many models, POC sinking and remineralization in the mesopelagic is simulated with an explicit sinking velocity coupled with a first-order remineralization rate coefficient (Dinauer et al., 2022) while other models use an implicit treatment with specified empirical power-law or exponential vertical remineralization curves (e.g., Martin et al., 1987). Velocities, rate coefficients, and remineralization curves may be further modulated by size class, depth, particulate mineral composition, or subsurface temperature or oxygen concentration (Laufkötter et al., 2016; Lima et al., 2014).

Here we focus on simulated export via gravitational particle sinking, which is incorporated in virtually all GOBMs in some form. Observation-based estimates of the global export flux have a large range (5–12 Pg C yr^{-1}; Siegel et al., 2016), which is almost identical to the range in export estimates for the modern-day era simulated by coupled climate models (4.5–12 Pg C yr^{-1}; Henson et al., 2022); that is, the observation-based estimates of export flux provide a poor constraint for biogeochemical models. Because of differences in model climate responses and parameterizations of the ocean biological carbon pump, substantial uncertainties also plague projections of future changes in export flux in response to climate change. For example, Henson et al. (2022) found a large inter-model spread in projected changes in export flux by 2100 between +0.16 and −1.98 Pg C yr^{-1} (+1.8 to −41%) under the high-emission SSP5-8.5 scenario.

Much of the export flux of organic carbon from the euphotic zone, taken here as the downward flux through 100 m (F_{100}), is consumed by respiration in the mesopelagic zone (100–1,000 m). The diverse mechanisms for vertical transport and remineralization of organic matter in the mesopelagic are only partially captured in models (Fennel et al., 2022). A steep decline with depth in the gravitational sinking flux of particles is well documented from mid-depth sediment traps (e.g., Dinauer et al., 2022; Lima et al., 2014; Lutz et al., 2007), but the exact processes involved are less well quantified and may include physical and biological particle fragmentation (Briggs et al., 2020) as well as particle consumption and repackaging by zooplankton (Stukel et al., 2019). Particle fluxes and the depth-scale of remineralization are affected by particle composition, size, density, and sinking speeds. Particles can vary widely from small, slowly sinking dead cells and detrital material, to large marine snow aggregates with enhanced sinking speeds from captured ballast material, to large rapidly sinking fecal pellets (Lam et al., 2011; Omand et al., 2020). Vertical migrators transport organic carbon downward from the euphotic zone into the mesopelagic zone, respiring CO_2 and releasing fecal pellets at depth (Archibald et al., 2019). Sinking particle fluxes and mesopelagic biological processes are typically not modeled in great mechanistic detail in contemporary GOBMs, and often relatively simplistic empirical relationships such as variants of the Martin power-law flux curve (Martin et al., 1987) are used in place of explicit representation of the processes controlling mesopelagic flux attenuation.

The proportion of sinking exported POC that survives remineralization in the mesopelagic zone to reach depths >1,000 m is referred to as the transfer efficiency, given here as the ratio of sinking fluxes at 100 and 1,000 m ($E_{1000/100}$). POC reaching 1,000 m depth is remineralized below the main thermocline, and the remineralized CO_2 is likely sequestered on timescales of >100 years from the atmosphere (Siegel et al., 2021). There is currently little consensus on the global magnitude or spatial patterns of transfer efficiency, with some approaches suggesting that $E_{1000/100}$ is high at high latitudes and low at low latitudes (DeVries & Weber, 2017; Marsay et al., 2015; Weber et al., 2016), whilst others imply the opposite pattern (Dinauer et al., 2022; Guidi et al., 2015; Henson et al., 2012; Lam et al., 2011; Mouw et al., 2016b). A variety of approaches have been used to generate these estimates, including paired in situ observations of ^{234}Th-derived export flux and deep sediment trap flux (Henson et al., 2012), vertical profiles of flux from drifting sediment traps (Marsay et al., 2015), or inverting the observed nutrient and/or oxygen distributions using an inverse model (Cram et al., 2018; DeVries & Weber, 2017; Weber et al., 2016). The differing approaches and the time and space scales that they integrate are likely significant sources of the uncertainty in global $E_{1000/100}$ patterns. In CMIP6 models, there are substantial differences in both the pre-industrial mean $E_{1000/100}$ (varying from 3% to 25% across models) and its response to 21st century climate change, with projections showing both increases and decreases in $E_{1000/100}$ over time (Wilson et al., 2022).

Early model skill assessments relied heavily on model-data comparisons to transient tracers, ocean physics, and sub-surface nutrient and oxygen fields that reflect the imprint of biological pump fluxes and ocean circulation (e.g., Doney et al., 2004; Matsumoto et al., 2004; Najjar et al., 2007). However, observational constraints on the ocean biological carbon pump have advanced considerably since the early global 3-D ocean biogeochemical modeling efforts (e.g., Bacastow & Maier-Reimer, 1990; Maier-Reimer, 1993). Global-scale data compilations of primary production, surface export and mesopelagic sinking carbon fluxes are now available based on a wealth of satellite remote sensing, sediment traps, and geochemical methods (e.g., Henson et al., 2012; Mouw et al., 2016a). Past model-data skill assessments using multi-model ensembles have highlighted differences in simulated ocean biological carbon pump patterns, magnitudes, and mechanisms and identified model biases relative to admittedly imperfect observational estimates (Laufkötter et al., 2015, 2016). This study expands on these past assessment efforts of the ocean biological carbon pump to include the current generation of GOBMs compiled for RECCAP2 (DeVries et al., 2023).

The objective of this study is to characterize a global-scale biological carbon pump from RECCAP2 models and compare the simulation results with observation-based metrics. The focus is on the spatial patterns and global-integrated rates from the multi-model ensemble mean taking into consideration inter-model spread. Key metrics include export of sinking POC from the surface euphotic zone and the efficiency of POC transfer through the mesopelagic ocean, both of which are central to ocean carbon storage. Based on identified model-observation and inter-model differences, we also provide guidance for future GOBM evaluations and development that could include targeted, more detailed analyses of dynamics and biases within individual RECCAP2 models.

2. Methods and Data

2.1. RECCAP2 Model Simulations and Observational Data Products

This study leveraged a collection of ocean simulation and observational data sets, outlined in Table 1, assembled for RECCAP2 following standardized protocols and data reporting for numerical and observation-based pCO_2 products (DeVries et al., 2023; Müller, 2023; RECCAP2 Ocean Science Team, 2022). The RECCAP2 ocean data sets included monthly surface and annual ocean interior output for the contemporary period from more than a dozen GOBM hindcast simulations, including both forward and data-assimilated models, along with observation-based surface ocean pCO_2 interpolation products. Many of the models included in the RECCAP2 suite have been used in the Global Carbon Project to assess the ocean carbon sink (Friedlingstein et al., 2022; Hauck et al., 2020). Table 2 presents a summary of the ecosystem components and parameterizations used in the RECCAP2 ocean biogeochemical models. Here, we present model results for 1985 to 2018 from RECCAP2 simulation A, which was forced with historical atmospheric reanalysis data and increasing atmospheric CO_2, and hence represents both steady-state and variable climate processes and both natural, pre-industrial carbon fluxes and anthropogenic carbon fluxes caused by rising atmospheric CO_2 (DeVries et al., 2023).

Spatial 2D model output and pCO_2 interpolation products were provided to RECCAP2 with $1° \times 1°$ resolution at monthly time steps, and 3D model output was resolved at annual time steps. All estimates derived in this study were computed on a $1° \times 1°$ grid. Global multi-model ensembles, spatial integrals and averages were computed as needed from the gridded results of the GOBMs in Table 1 averaged over 1995–2018 using the RECCAP2 model simulation A outputs; the data assimilation models (ECCO-Darwin and SIMPLE-TRIM) were excluded from the multi-mean ensembles. For the aggregation to sub-basin ocean regions, ocean biomes based on Fay and McKinley (2014) were used in most instances to facilitate consistent regional intercomparison across RECCAP2 studies (e.g., Hauck et al., 2023). Longhurst provinces (Figure S1 in Supporting Information S1; Reygondeau et al., 2013) were additionally used in some of the biological pump model-observational comparisons to be consistent with one of the key observational data synthesis products (Mouw et al., 2016a). The notation and units for the biological, chemical and physical variables used in this study are described in Table 3. More details on the RECCAP2 ocean data sets can be found in DeVries et al. (2023).

We also used an observational compilation of surface ocean export production and sinking POC flux combined with satellite ocean color data products for primary production synthesized by Mouw et al. (2016a) and as aggregated to Longhurst regional provinces by Mouw et al. (2016b). The full data set includes over 15,000 individual sediment trap and ^{234}Th POC flux measurements at 673 locations, combined with satellite-derived estimates of NPP. Chlorophyll measurements collected from the SeaWiFS sensor on the OrbView-2 ocean color satellite, spanning from August 1997 to December 2010, were used to derive NPP using the vertically generalized

Table 1
Description of RECCAP2 Global Ocean Biogeochemical Models, Global Data-Assimilated Models, and Observation-Based Products Used in This Study

Biogeochemical models	Data range	References
CCSM-WHOI	1958–2017	Doney et al. (2009)
CESM-ETHZ	1980–2018	Lindsay et al. (2014) and Yang and Gruber (2016)
CNRM-ESM2-1	1980–2018	Séférian et al. (2019, 2020) and Berthet et al. (2019)
EC-Earth3	1980–2018	Aumont et al. (2015) and Döscher et al. (2022)
FESOM-REcoM-LR	1980–2018	Hauck et al. (2013, 2020)
MPIOM-HAMOCC	1980–2018	Ilyina et al. (2013) and Mauritsen et al. (2019)
MOM6-Princeton	1980–2018	Liao et al. (2020) and Stock et al. (2020)
MRI-ESM2-1	1980–2018	Urakawa et al. (2020) and Tsujino et al. (2017)
NorESM-OC1.2	1980–2018	Schwinger et al. (2016)
NEMO-PlankTOM12.1	1980–2018	Le Quéré et al. (2016) and Wright et al. (2021)
ORCA1-LIM3-PISCES	1980–2018	Aumont et al. (2015)
Data-assimilated models		
ECCO-Darwin	1995–2018	Carroll et al. (2020, 2022)
SIMPLE-TRIM	Climatology	DeVries and Weber (2017)
pCO_2 interpolation products		
CMEMS-LSCE-FFNN	1985–2018	Chau et al. (2022)
JenaMLS	1985–2018	Rödenbeck et al. (2013, 2022)
MPI-SOMFFN	1982–2018	Landschützer et al. (2016)
NIES-ML3	1980–2020	Zeng et al. (2022)
OceanSODA-ETHZ	1985–2018	Gregor and Gruber (2021)
LDEO_HPD	1985–2018	Gloege et al. (2022)
UOEX_Wat20	1985–2019	Watson et al. (2020)
World Ocean Atlas		
Oxygen and AOU	Climatology	Garcia et al. (2019)
Biological carbon pump metrics		
Net primary production, export production, and sinking POC flux	Climatology	Mouw et al. (2016a, 2016b)

Note. For more details see Tables S1 and S2 in Supporting Information S1 in DeVries et al. (2023). The World Ocean Atlas (WOA) data set was also used in the model-data evaluation.

production model (Behrenfeld & Falkowski, 1997) on an equal-area grid with 9-km resolution. The climatology in Mouw et al. (2016a) used an interpolation approach to combine the satellite timeseries and short-deployment (<30 days trap cup intervals) sediment trap POC flux measurements at overlapping locations. Over 43% of the POC flux measurements were collected after 1997, overlapping with the satellite record. For each POC flux location, median monthly values are computed and binned into biogeochemical Longhurst provinces for the climatology. The POC flux climatology also has a depth dimension, with depth bins centered at 20 m for a near-surface layer, in 50 m intervals in the upper thermocline, and in 200 m intervals from 500 to 5,000 m.

2.2. Ocean Biological Pump and Biogeochemical Metrics

Our analysis utilized biogeochemical model estimates of vertically integrated NPP and export fluxes of sinking POC across a shallow surface at the approximate base of the euphotic zone (100 m, F_{100}) and at the base of the main thermocline (1,000 m, F_{1000}). Note that the 1,000 m fluxes were not provided for all models (see Figure 2c), and therefore the ensemble means for F_{100} and F_{1000} were constructed from different subsets of RECCAP2 simulations. The export ratio, $E_{100/NPP}$, was computed as the ratio of POC sinking flux at 100 m divided by vertically integrated net primary production:

Global Biogeochemical Cycles

10.1029/2024GB008156

Table 2
Summary Description of RECCAP2 Global Ocean Biogeochemical Models Divided Into Euphotic and Mesopelagic Processes

Biogeochemical model				
Euphotic zone	Nutrient	Phytoplankton types	Phyto growth	Zooplankton
CCSM-WHOI	P, N, Fe, Si	Small, diatom, diazotroph	I, T, Chl, Fe/C, Si/C	Single adaptive class
CESM-ETHZ	P, N, Fe, Si	Small, diatom, diazotroph	I, T, Chl, Fe/C, Si/C	Single adaptive class
CNRM-ESM2-1	P, N, Fe, Si	Nano-, diatom	I, T, Chl, Fe/C, Si/C	Micro-, meso-
EC-Earth3	P, N, Fe, Si	Nano-, diatom	I, T, Chl, Fe/C, Si/C	Micro-, meso-
FESOM-REcoM-LR	N, Fe, Si	Small, diatom	I, T, N/C	Single class
MPIOM-HAMOCC	P, N, Fe, Si	Bulk phyto, diazotroph	I, T	Single class
MOM6-Princeton	P, N, Fe, Si	Small, large, diazotroph	I, T, Fe/C, Si/C	Small, medium, large
MRI-ESM2-1	P, N	Bulk phyto, diazotroph	I, T	Single class
NorESM-OC1.2	P, N, Fe, Si	Bulk phyto, diazotroph	I, T	Single class
NEMO-PlankTOM12.1	P, N, Fe, Si	Pico-, diatom, diazotroph, coccolithophores, mixed, *Phaeocystis*	I, T, Chl, Fe/C	Proto-, meso-, macro-, and jellyfish (+bacteria)
ORCA1-LIM3-PISCES	P, N, Fe, Si	Nano-, diatoms	I, T, Chl, Fe/C, Si/C	Micro-, meso-

Mesopelagic	Detrital POC	POC sinking	Remineralization rate
CCSM-WHOI	Free, mineral associated	Implicit	Exponential: depth, T, mineral
CESM-ETHZ	Free, mineral associated	Implicit	Exponential: depth, T, mineral
CNRM-ESM2-1	Small, large	Explicit: depth for large	T, O_2
EC-Earth3	Small, large	Explicit: depth for large	T, O_2
FESOM-REcoM-LR	Single class	Explicit: depth	T
MPIOM-HAMOCC	Single class	Explicit: depth	O_2
MOM6-Princeton	Free, mineral associated	Implicit	Exponential: depth, T, mineral
MRI-ESM2-1	Single class	Explicit: depth	Power law: depth
NorESM-OC1.2	Single class	Explicit	O_2
NEMO-PlankTOM12.1	Small, large	Explicit: N mineral for large	
ORCA1-LIM3-PISCES	Small, large	Explicit	T

Note. See Table 1 for the RECCAP2 model references. The upper section includes columns for prognostic nutrients and micro-nutrients, phyto- and zoo- Plankton Functional Types (PFTs), and phytoplankton growth terms in addition to nutrients from irradiance (I), temperature (T), and variable cell composition relative to carbon biomass. The lower section includes columns for forms of sinking particulate organic carbon (POC), treatment of POC sinking, and factors influencing the parameterization of remineralization rate. For models with implicit sinking, the form of the vertical remineralization curve is given. Note that the specific functional forms and numerical parameter values vary across models even for conceptually similar parameterizations. Note that a list of PFTs and trophic levels alone does not fully capture the realized food-web structure and ecosystem dynamics (Sailley et al., 2013).

Table 3
Glossary and Description of Modeled, Observed, and Derived Variables Including Notation and Units

Variable name	Units	Output frequency	Description
2D or surface ocean properties			
pCO_2	µatm	Monthly	Surface ocean pCO_2
NPP	mol C m^{-2} yr^{-1}	Monthly	Vertically integrated net primary production of organic carbon
F_{100}	mol C m^{-2} yr^{-1}	Monthly	POC sinking flux at 100 m
F_{1000}	mol C m^{-2} yr^{-1}	Monthly	POC sinking flux at 1,000 m
3D or Interior ocean properties			
T	°C	Annual	Seawater potential temperature
S	–	Annual	Salinity (PSS-78)
F_{3D}	mol C m^{-2} yr^{-1}	Annual	3D field of POC sinking flux
O_2	mol O_2 m^{-3}	Annual	Dissolved oxygen concentration
Derived variables			
$E_{100/NPP} = F_{100}/NPP$	–	Monthly	Surface Export Ratio
$E_{1000/100} = F_{1000}/F_{100}$	–	Monthly	Mesopelagic Transfer Efficiency
$E_{1000/NPP} = F_{1000}/NPP$	–	Monthly	Surface to Deep-sea Export Efficiency
AOU	µmol kg^{-1}	Monthly	Apparent oxygen utilization

$$E_{100/\mathrm{NPP}} = \frac{F_{100}}{\mathrm{NPP}} \tag{1}$$

The transfer efficiency across the 1,000 m depth horizon, $E_{1000/100}$, was similarly computed as the ratio of sinking POC fluxes at 100 and 1,000 m:

$$E_{1000/100} = \frac{F_{1000}}{F_{100}} \tag{2}$$

A depth of 1,000 m is taken as an approximate boundary between the main thermocline with ventilation time-scales of years to decades and the deep ocean with time-scales of a century and longer (Siegel et al., 2021).

The relationship between the biological pump and the inorganic CO_2 system was examined by partitioning the seasonal variability in surface seawater pCO_2 into thermal and non-thermal components following Takahashi et al. (2002). We refer readers interested in a thorough analysis of RECCAP2 CO_2 system seasonality to Rodgers et al. (2023). The temperature effect on pCO_2 was calculated for isochemical seawater using the approximation $\frac{\partial(\ln(pCO_2))}{\partial T} = 0.0423$ ($°C^{-1}$) from the experimental value from Takahashi et al. (1993). The seasonal cycle in monthly surface temperature anomalies relative to the annual mean surface temperature generated a corresponding seasonal variation in the thermal (temperature-dependent) pCO_2 component about the pCO_2 annual mean:

$$pCO_2^{\mathrm{thermal}} = (pCO_2)_{\mathrm{mean}} \times \exp[0.0423(T_{\mathrm{monthly}} - T_{\mathrm{mean}})] \tag{3}$$

Ocean hindcast simulations are typically forced by satellite-derived radiative fluxes, precipitation estimates, and atmospheric reanalysis surface winds, air temperatures, and humidity values that are used in the turbulent bulk flux formula to compute air-sea momentum flux, sensible and latent heat fluxes, and evaporation (Large & Yeager, 2009; Large et al., 1997). Hindcasts typically capture quite well the seasonal cycle of sea surface temperature because the atmospheric reanalysis products used in the bulk flux formula effectively contain information on the observed ocean surface temperature record (Doney et al., 2007); the same model-data agreement transfers to the thermal pCO_2 seasonal component. The non-thermal pCO_2 component was computed by

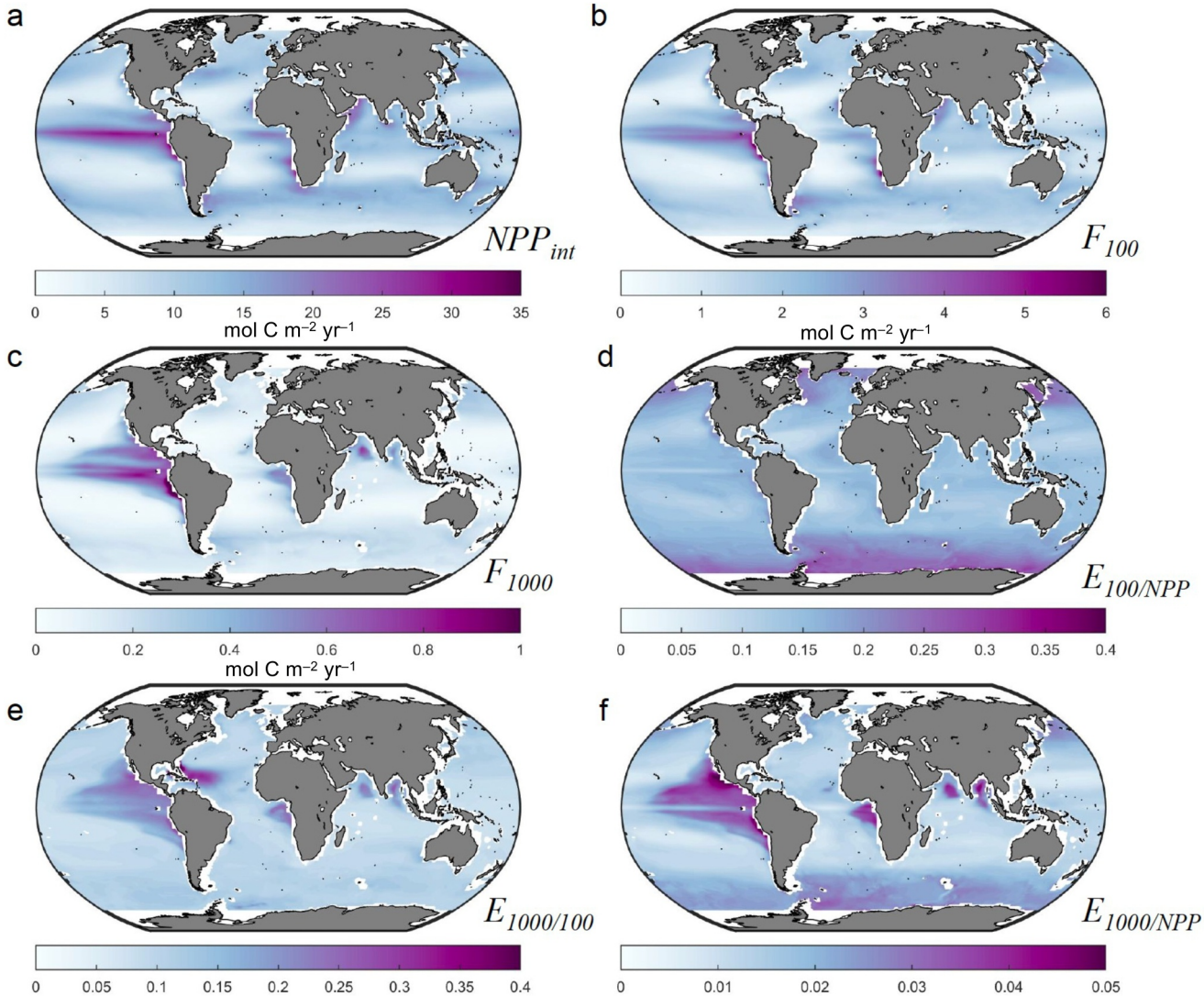

Figure 1. Multi-model ensemble averages of biological pump metrics from RECCAP2 model simulations. Maps of annual mean (a) integrated net primary productivity NPP, (b) particulate organic carbon export fluxes at 100 m (F_{100}), and (c) 1,000 m (F_{1000}), all in mol C m^{-2} yr^{-1}. Ensemble mean (d) export efficiency ratio $E_{100/NPP} = F_{100}$/NPP (Equation 1), (e) mesopelagic transfer efficiency at 1,000 m $E_{1000/100} = F_{1000}/F_{100}$ (Equation 2), and (f) export efficiency to the deep ocean $E_{1000/NPP} = F_{1000}$/NPP, all ratios unitless.

subtracting the thermal component from the monthly pCO_2 values, and the seasonal amplitude $\Delta pCO_{2,non\text{-}thermal}$ was calculated as the seasonal peak-to-trough difference. The non-thermal pCO_2 component reflects seasonal variations in DIC and alkalinity from biological organic and inorganic carbon production and remineralization, air-sea CO_2 gas exchange, and physical transport and mixing. Note that the seasonal phasing of the non-thermal pCO_2 component can be distinct from the phasing of the total pCO_2 cycle. This is especially the case in the low latitudes, where the thermal component dominates the seasonal cycle (Landschützer et al., 2018; Rodgers et al., 2023; Takahashi et al., 1993).

We also computed apparent oxygen utilization (AOU) using modeled dissolved oxygen, salinity, and potential temperature fields. Modeled average AOU at 100 m (AOU_{100}) and 1,000 m depth (AOU_{1000}) were found using nearest depth bins in model products (bins centered within 50 m of depths). The simulated AOU fields are compared against the World Ocean Atlas (WOA) data product (Garcia et al., 2019).

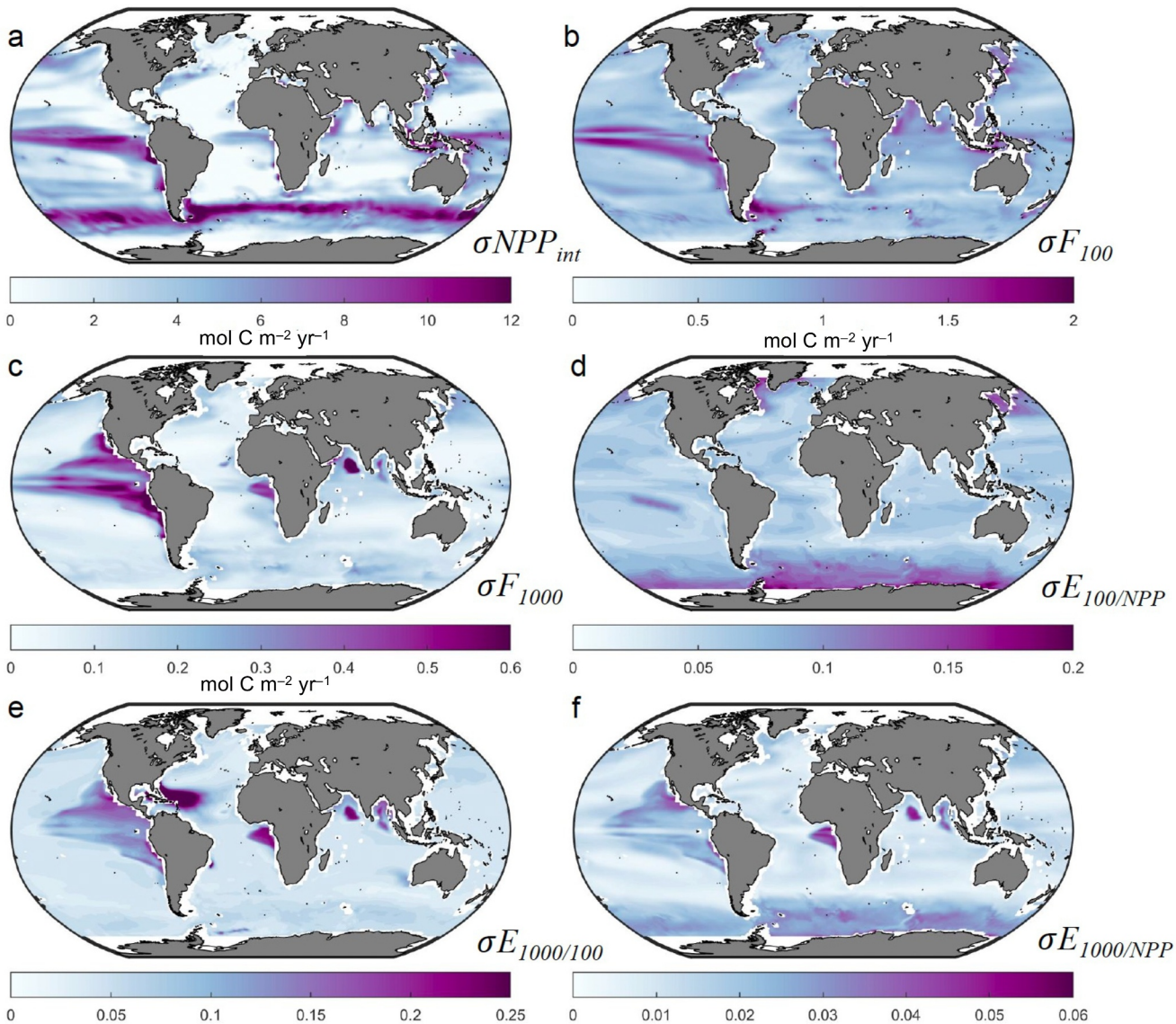

Figure 2. Maps of within-ensemble standard deviation of biological pump metrics. Standard deviations across model ensemble members are computed relative to the average model ensemble presented in Figure 1 for: (a) vertically integrated primary productivity σ_{NPP}, (b) particulate organic carbon export fluxes at 100 m σF_{100}, and (c) 1,000 m σF_{1000}, all in mol C m^{-2} yr^{-1}, and (d) surface export efficiency ratio $E_{100/NPP} = F_{100}$/NPP, (e) mesopelagic transfer efficiency at 1,000 m $E_{1000/100} = F_{1000}/F_{100}$, and (f) export efficiency to the deep ocean $E_{1000/NPP} = F_{1000}$/NPP, all ratios unitless.

3. Results

3.1. Simulated Ocean Biological Carbon Pump Metrics

Global spatial fields of present-day biological carbon pump variables are displayed in Figure 1 for the RECCAP2 model ensemble mean with the corresponding ensemble standard deviation in Figure 2. Biome-scale ensemble-mean averages and within-ensemble standard deviation values for the biological pump metrics are reported in Table 4 using the standard RECCAP2 biomes by ocean basin (Figure S1 in Supporting Information S1; Fay & McKinley, 2014).

The simulated annual mean NPP and export flux from sinking POC (F_{100}) (Figures 1a and 1b) exhibited large geographic variations, with annual-mean NPP ranging on biome scales (Table 4) from 8 to 21 mol C m^{-2} yr^{-1} and F_{100} ranging from 1.0 to 2.9 mol C m^{-2} yr^{-1}. The simulated spatial patterns reflect euphotic zone temperature,

Table 4
Model Ensemble Averages and Standard Deviations of Biological Pump Parameters by RECCAP2 Regional Biomes (Figure S1 in Supporting Information S1) (See Also Figure 1) Grouped as Sub-Polar Seasonally Stratified (SPSS), Sub-Tropical Seasonally Stratified (STSS), Sub-Tropical Permanently Stratified (STPS), Equatorial (EQU), and Mediterranean (MED)

	NPP	F_{100}	F_{1000}	$E_{100/NPP}$	$E_{1000/100}$	$E_{1000/NPP}$
SPSS						
N. Pacific	11.89 ± 4.81	2.21 ± 0.65	0.307 ± 0.263	0.206 ± 0.076	0.124 ± 0.071	0.018 ± 0.012
N. Atlantic	9.30 ± 3.00	1.77 ± 0.65	0.177 ± 0.156	0.211 ± 0.075	0.116 ± 0.060	0.014 ± 0.009
Southern	9.24 ± 6.64	1.59 ± 0.60	0.197 ± 0.119	0.213 ± 0.091	0.132 ± 0.071	0.023 ± 0.025
STSS						
N. Pacific	13.53 ± 3.68	2.04 ± 0.70	0.206 ± 0.117	0.161 ± 0.040	0.114 ± 0.049	0.014 ± 0.006
N. Atlantic	12.98 ± 3.28	1.93 ± 0.54	0.165 ± 0.069	0.162 ± 0.049	0.099 ± 0.036	0.014 ± 0.006
Southern	13.91 ± 5.02	2.12 ± 0.39	0.222 ± 0.087	0.173 ± 0.053	0.109 ± 0.040	0.016 ± 0.009
STPS						
N. Pacific	8.92 ± 3.24	1.18 ± 0.61	0.177 ± 0.102	0.131 ± 0.047	0.132 ± 0.049	0.017 ± 0.010
N. Atlantic	7.70 ± 2.37	0.97 ± 0.44	0.092 ± 0.057	0.121 ± 0.051	0.140 ± 0.097	0.013 ± 0.008
S. Atlantic	9.78 ± 2.16	1.33 ± 0.41	0.138 ± 0.090	0.130 ± 0.043	0.104 ± 0.040	0.012 ± 0.008
Indian	16.67 ± 4.75	2.25 ± 0.85	0.284 ± 0.162	0.143 ± 0.035	0.130 ± 0.063	0.016 ± 0.008
EQU						
W. Pacific	11.03 ± 5.31	1.44 ± 1.06	0.10 ± 0.078	0.134 ± 0.059	0.089 ± 0.050	0.013 ± 0.011
E. Pacific	21.16 ± 5.16	2.91 ± 0.74	0.542 ± 0.288	0.151 ± 0.043	0.178 ± 0.086	0.027 ± 0.015
Atlantic	14.33 ± 4.71	1.94 ± 0.65	0.272 ± 0.137	0.145 ± 0.039	0.140 ± 0.043	0.019 ± 0.010
MED	9.21 ± 3.71	1.34 ± 0.79	0.074 ± 0.062	0.141 ± 0.060	0.119 ± 0.107	0.011 ± 0.008

Note. Table includes annual means and standard deviations for vertically integrated net primary productivity NPP, particulate organic carbon export fluxes at 100 m F_{100}, and 1,000 m depth F_{1000}, all in mol C m^{-2} yr^{-1}, and average surface export efficiency ratio $E_{100/NPP} = F_{100}/NPP$, mesopelagic transfer efficiency at 1,000 m $E_{1000/100} = F_{1000}/F_{100}$, and export efficiency to the deep ocean $E_{1000/NPP} = F_{1000}/NPP$, all ratios unitless. Ensemble were not computed for the small, high-latitude polar ice biomes due to noisy and/or missing data across the full ensemble.

nutrient supply, and grazing and loss rates that govern phytoplankton standing stock in the models (Falkowski et al., 1998; Laufkötter et al., 2015, 2016). The imprint of nutrient supply was particularly evident in the elevated NPP and export fluxes found in equatorial and coastal upwelling regions, western boundary currents, and mid-latitude bands of deep seasonal mixing (Figures 1a and 1b). Within-ensemble standard deviations (σ) of NPP and F_{100} were elevated in the equatorial band, and high σ_{NPP} values were also found in the Southern Ocean, indicating substantial model disagreement within the ensemble (Figures 2a and 2b). Biome-scale σ_{NPP} values ranged from 2.0 to 6.6 mol C m^{-2} yr^{-1}. The lowest relative spread (σ_{NPP}/NPP) was 0.22 in the permanently stratified subtropical South Atlantic, while the highest relative spread was 0.72 in the subpolar Southern Ocean. The biome-scale σ_{F100} values varied from 0.4 to >1.0 mol C m^{-2} yr^{-1} with the largest within-ensemble variation occurring in the western equatorial Pacific.

The local POC sinking flux at the base of the mesopelagic (F_{1000}) ranged at the biome scale from 0.09 to 0.54 mol C m^{-2} yr^{-1} with broadly similar patterns to F_{100}, though with some notable exceptions such as the high F_{1000} values in tropical low-oxygen zones in the eastern tropical Pacific and Arabian Sea (Figure 1c). Note the roughly half to full order of magnitude decline in scale in Figure 1 from NPP to F_{100} and then F_{100} to F_{1000}. This indicates first that the bulk of simulated NPP is recycled within the euphotic zone above 100 m, rather than exported as sinking POC flux, and second that most of the sinking POC flux at 100 m is remineralized in the mesopelagic, rather than reaching the deep ocean below 1,000 m. As for NPP and F_{100}, some correspondence was found for the spatial patterns of ensemble-means F_{1000} and σ_{F1000}. The highest biome-scale σ_{F1000} values of 0.26–0.29 mol C m^{-2} yr^{-1} occurred in the North Pacific and eastern equatorial Pacific (Figure 2; Table 4).

The fraction of NPP exported across 100 m or export ratio ($E_{100/NPP}$, Figure 1d; Table 4) varies at the biome scale in the ensemble mean from 0.12 to 0.21 with elevated values in high latitudes. The spatial patterns for within-

ensemble $E_{100/NPP}$ standard deviation (Figure 2d) mirror that of the mean $E_{100/NPP}$ with biome-mean standard deviations of 0.035–0.060 in most biomes and up to 0.091 in the sub-polar Southern Ocean biome where there is more within-ensemble model spread.

The ensemble-mean transfer efficiency through the mesopelagic, $E_{1000/100}$ (Figure 1e; Table 4), exhibited background levels at the biome-scale of 0.09–0.14 for most biomes and ranged as high as 0.18 in the eastern equatorial Pacific biome; sub-biome regional values up to 0.3 occurred in the eastern tropical Pacific, western and eastern tropical Atlantic, and Arabian Sea and Bay of Bengal. Some ocean biogeochemical models reduce subsurface POC remineralization in low-oxygen zones, using a parameterization based on local oxygen concentrations, driving higher $E_{1000/100}$ values in low-oxygen regions such as the eastern tropical Pacific, Arabian Sea and Bay of Bengal. Furthermore, POC flux mineral ballasting from Saharan dust deposition, prescribed as an external forcing, is likely an important contributor in at least some models (CCSM-WHOI and CESM-ETHZ) to high $E_{1000/100}$ in the western tropical Atlantic (Lima et al., 2014). The ensemble $E_{1000/100}$ standard deviation (Figure 2e) generally followed $E_{1000/100}$ with particularly large $\sigma E_{1000/100}$ values up to 0.3 in the western tropical Atlantic reflecting differences across models in the parameterization of POC sinking in the presence of desert dust. The metric $E_{1000/NPP}$ (Figure 1f), combining surface export and mesopelagic transfer efficiencies, had generally similar spatial patterns to $E_{1000/100}$ but with lower values, reflecting the small fraction of NPP that sinks below 1,000 m and is sequestered in the deep ocean. More than a factor of two variation was found for metric $E_{1000/NPP}$ across biomes (0.012–0.027) with large within-ensemble variation for some biomes where the standard deviation approached or exceeded the ensemble mean.

To illustrate differences among the models making up the RECCAP2 multi-model ensemble, global integrals of the annual average biological pump metrics are displayed in Figure 3. A box-whisker plot is shown for each model ensemble member quantifying the interannual variability for each model for the RECCAP2 reporting period (1985–2018). Note that some RECCAP2 models did not report F_{1000}, resulting in missing estimates for $E_{1000/100}$ and $E_{1000/NPP}$. Some models stood out as either anomalously low (e.g., FESOM-REcoM-LR for NPP) or high (e.g., NEMO-PlankTOM12.1 for F_{100}) relative to the other RECCAP2 ensemble members, though inter-model agreement alone is not necessarily a robust indicator of model skill (see Section 3.2). For global $E_{100/NPP}$, the models were roughly split into low (0.10–0.12) and high (0.16–0.19) groups (Figure 3d). Global F_{1000}, $E_{1000/100}$, and $E_{1000/NPP}$ varied widely for the smaller number of available models (Figures 3c, 3e, and 3f).

3.2. Model-Observational Comparisons

The global ocean biological carbon pump metrics from the RECCAP2 multi-model ensemble were compared against corresponding literature values in Table 5 and Figure 4. The RECCAP2 multi-model ensemble global-integrated NPP value, 41.5 ± 9.0 Pg C yr^{-1}, was at the lower end of literature estimates (43.5–68 Pg C yr^{-1}), and the inter-quartiles have limited overlap. Similarly, global-integrated F_{100} from the multi-model ensemble of 6.08 ± 1.17 Pg C yr^{-1} was lower than the mean of the literature estimates of sinking POC flux (~8 Pg C yr^{-1}, range 4–13 Pg C yr^{-1}), though the inter-quartiles overlapped substantially because of the large range in observation-based estimates. The global-integrated model ensemble F_{1000} value of 0.65 ± 0.24 Pg C yr^{-1} fell near one low estimate of 0.66 Pg C yr^{-1} (Henson et al., 2012) and below two other literature estimates of 1.1 Pg C yr^{-1}. The global multi-model ensemble-mean export and transfer efficiencies, $E_{100/NPP}$ (0.154 ± 0.026) and $E_{1000/100}$ (0.122 ± 0.041), were within the range of literature values after removing the high $E_{100/NPP}$ values (0.3 and 0.38) from Laws et al. (2000) and acknowledging one low outlier model for global $E_{1000/100}$ (~0.05; CCSM-WHOI; Figure 3e).

The wide range of literature estimates reflects differences in measurement methodologies, biases, and uncertainties in the data sets used for biological carbon pump metric estimation, as well as uncertainties introduced by data sampling biases, aggregation, time/space interpolation and modeling approaches. At global scales, in situ observational sampling for some variables remains sparse and regionally patchy, and satellites, empirical relationships, and numerical models have been used to gap-fill for global-scale product generation. For example, even with field data sets available for ocean NPP based on ^{14}C uptake incubation studies, satellite remote sensing has been required to create uniform global NPP products, which have been calibrated/validated against ^{14}C NPP field data.

A variety of in situ methods have been used to estimate surface ocean export flux estimates (~F_{100}) including drifting sediment traps and ^{234}Th deficits. To derive global-scale fields of export, extrapolation from the limited in

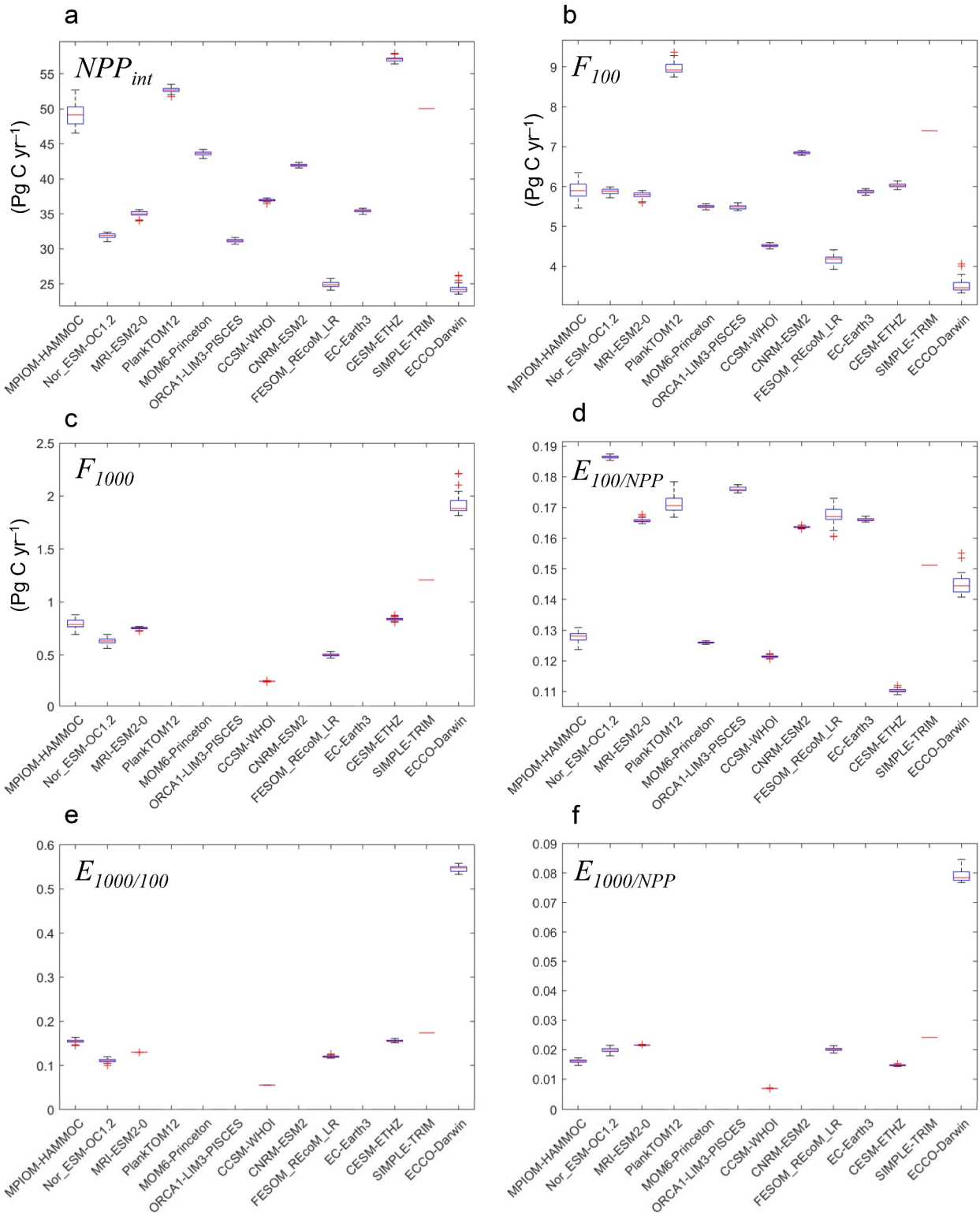

Figure 3.

situ data is required, which generates uncertainties in the derived estimates due to the underlying data sparsity (Henson et al., 2024). Typically, satellite data are used to build an empirical relationship between flux and readily derived variables, such as sea surface temperature or chlorophyll concentration. Other approaches include merging satellite data with food-web models (e.g., Siegel et al., 2014). Observation-based global F_{1000} estimates have been generated from sediment trap data (Mouw et al., 2016a), and estimates of both global F_{100} and F_{1000} have been derived from inverse and data-assimilation ocean models (e.g., DeVries & Weber, 2017; Nowicki et al., 2022).

The biological carbon pump model comparison to observation-based estimates was extended in Figure 5 to a regional level using the POC flux estimates from sediment trap and ^{234}Th deficit observations from Mouw et al. (2016a) as aggregated by Mouw et al. (2016b) into monthly climatological values for Longhurst biogeographic provinces (Figure 5). The Mouw et al. (2016a) date set aggregates the limited available field data that is often spatially sparse and locally high frequency with considerable mesoscale variability, some of which may be aliased into monthly and province scale averages. Therefore, robust uncertainty estimates are not available for the Mouw et al. (2016b) observational climatology. The variations across the RECCAP2 models are displayed as box-whisker plots. The members of the model ensemble exhibited a wide range of NPP, F_{100} and F_{1000} values for many provinces, but the multi-model ensemble interquartiles still overlapped the observational climatology for only about half of the provinces. The substantial model-observational offsets indicate recurring regional differences consistent across multiple models in the RECCAP2 ensemble; these disagreements could be targets for future ocean biogeochemical model development and analyses of observational sampling biases.

The model ensemble members also exhibited extreme model-data differences in some provinces where the observational climatology value falls outside the simulated range, including model outliers. The RECCAP2 models underestimated the strength of some biological carbon pump metrics, relative to the observational climatology, in polar and sub-polar provinces in the North Pacific (BERS, low NPP and F_{100}) and North Atlantic (NADR, low NPP); and in equatorial upwelling provinces in the Arabian Sea (ARAB, low NPP), Eastern Equatorial Pacific (PEQD, low F_{100}) and Guianas coast (GUIA, low F_{1000}; note that this is a small, productive region that may not be well represented in global-scale models). The model ensemble overestimated the biological pump in the South Pacific gyre (SPSG, high NPP and F_{100}), Indian monsoon gyre (MONS, high NPP and F_{100}), and Western Pacific subarctic gyres (PSAW, high F_{1000}).

3.3. Biological Pump Imprint on Ocean CO_2 System and Biogeochemistry

The ocean biological carbon pump imprints on surface and sub-surface biogeochemistry (see Section 1), and these effects were simulated in the RECCAP2 models. A strong positive mesopelagic AOU signal is generated by cumulative biological O_2 consumption along the ventilation paths of subsurface waters (Najjar et al., 2007). AOU fields thus integrate non-local, large-scale biogeochemical dynamics and physical resupply of O_2 from the surface. A key contributor to AOU is the remineralization of sinking POC flux in the mesopelagic, quantified by the large decline between F_{100} and F_{1000} and low transfer efficiency through the mesopelagic $E_{1000/100}$ (Figures 1 and 3; Tables 4 and 5). For the RECCAP2 model ensemble, there was generally good model-data agreement in the geographic pattern in AOU averaged over the mesopelagic (100–1,000 m) (Figure 6).

The model ensemble captured the regional AOU variation of <50 to >250 μmol kg^{-1} relative to WOA (grid-scale $R^2 = 0.942$; RMSE = 21.3 μmol kg^{-1}; mean model bias = +1.34 μmol kg^{-1}), with good agreement also on the scale of Longhurst provinces where the model-ensemble interquartile spans the observational data (Figure 5) for most of the subset of provinces (Figure 5) shown in Figure 6c. The RECCAP2 models did not exhibit a strong inter-model relationship between global mean AOU and F_{100} (not shown). A weak relationship between AOU and F_{100} across models arises because AOU is strongly influenced by the strength of model thermocline ventilation rates (e.g., Dutay et al., 2002; Matsumoto et al., 2004), which vary substantially across models (Terhaar et al.,

Figure 3. Boxplots showing median values, interannual interquartile ranges, and outliers (+ symbols when present) of biological pump metrics across the individual models in RECCAP2 (Table 1). Globally integrated, annual (a) net primary productivity NPP, (b) particulate organic carbon export fluxes at 100 m F_{100}, and (c) 1,000 m depth F_{1000}, all in Pg C yr^{-1}. Global and annual average (d) surface export efficiency ratio $E_{100/NPP} = F_{100}$/NPP (Equation 1), (e) mesopelagic transfer efficiency at 1,000 m $E_{1000/100} = F_{1000}/F_{100}$ (Equation 2), and (f) export efficiency to the deep ocean $E_{1000/NPP} = F_{1000}$/NPP, all ratios unitless. CCSM-WHOI output does not include the year 2018 and SIMPLE-TRIM does not simulate interannual variability. Transfer efficiency ratios are not given in panels e and f for models lacking the corresponding F_{1000} in the RECCAP2 database (PlankTOM12, MOM6-Princeton, ORCA1-LIM3-PICES, CNRM-ESM2, and EC-Earth3).

Table 5
Comparison of Literature-Based, Global Observation-Based Ocean Biological Carbon Pump Metrics With the RECCAP2 Model Ensemble Means and Within-Ensemble Standard Deviations

Net primary production NPP (Pg C yr^{-1})	References
43.5	VGPM Behrenfeld and Falkowski (1997)
52	CAFÉ Silsbe et al. (2016)
68	Carr (2002) and Carr et al. (2006)
49	Marra et al. (2003)
52	CbPM2 Behrenfeld et al. (2005)
52.9 ± 9.1	Observational mean and STD
41.5 ± 9.0	RECCAP2 model ensemble mean and STD
POC Export $\sim F_{100}$ (Pg C yr^{-1})	
4	Henson et al. (2012)
9.6	Dunne et al. (2007)
11.1–12.9	Laws et al. (2000)
5.7	Siegel et al. (2014)
9.6	Schlitzer (2000); inversion
9–13	Laws et al. (2011)
8.8 (7.3 at 100 m)	DeVries and Weber (2017); data assimilating
7.3 (6.4 at 100 m)	Nowicki et al. (2022)
8.20 ± 2.78	Observational mean and STD
6.08 ± 1.17	RECCAP2 model ensemble-mean and STD
POC Flux 1,000 m F_{1000} (Pg C yr^{-1})	
0.66	Henson et al. (2012)
1.1	DeVries and Weber (2017)
1.1	Nowicki et al. (2022)
0.95 ± 0.25	Observational mean and STD
0.65 ± 0.24	RECCAP2 model ensemble mean and STD
Export Ratio $\sim E_{100/NPP} = F_{100}/NPP$	
0.1	Henson et al. (2012)
0.19	Dunne et al. (2007)
0.3	Laws et al. (2000); food web
0.38	Laws et al. (2000); empirical
0.103	Siegel et al. (2014)
0.17	DeVries and Weber (2017)
0.13 (for POC only)	Nowicki et al. (2022)
0.18 (for POC + DOC + vertical migration)	Nowicki et al. (2022)
0.196 ± 0.106	Observational mean and STD
0.154 ± 0.026	RECCAP2 model ensemble mean and STD
Transfer flux efficiency $E_{1000/100} = F_{1000}/F_{100}$	
0.19	Henson et al. (2012)
0.13	DeVries and Weber (2017)
0.15	Nowicki et al. (2022)
0.157 ± 0.031	Observational mean and STD
0.122 ± 0.041	RECCAP2 model ensemble mean and STD

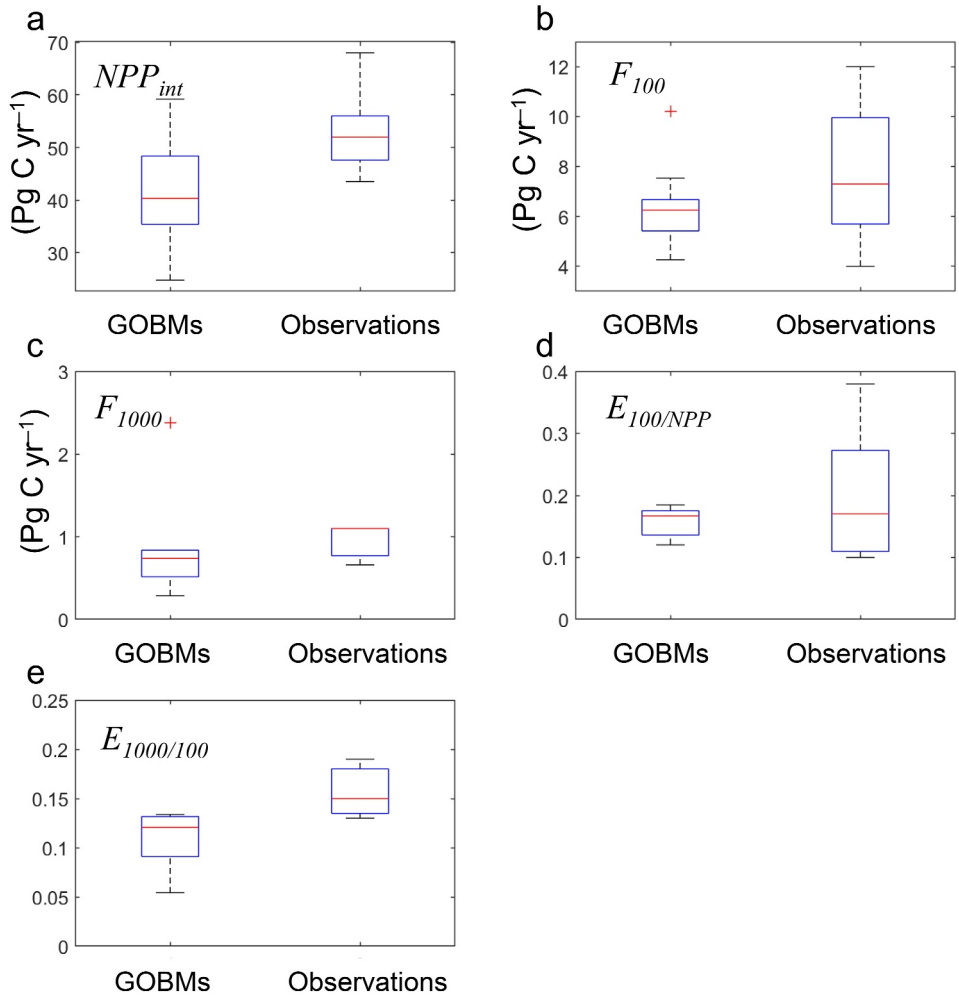

Figure 4. Box-whisker plots showing median values, interquartile ranges, and outliers (red plus symbol when present) of biological pump parameters from the RECCAP2 global ocean biogeochemical model (GOBM) ensemble (left) and observational estimates (right; Table 5). Global integrated, annual (a) net primary productivity NPP, (b) particulate organic carbon export fluxes at 100 m F_{100}, and (c) 1,000 m depth F_{1000}, all in Pg C yr^{-1} (note that the median line for F_{1000} is also the upper interquartile because two of the three observational estimates match). Global and annual average surface export efficiency ratio (d) $E_{100/NPP} = F_{100}$/NPP (Equation 1), and (e) mesopelagic transfer efficiency at 1,000 m $E_{1000/100} = F_{1000}/F_{100}$ (Equation 2), all ratios unitless.

2024). Model deep-ocean AOU was not evaluated because model spin-up time scales were too short for the simulations to reach steady-state (Séférian et al., 2019), an issue that also would affect simulated deep-ocean pre-industrial DIC (Mikaloff Fletcher et al., 2007). Some imprint of the observational fields used for model initial conditions could also be retained in the simulated mesopelagic AOU depending on the model spin-up procedure.

The simulated regional patterns and global integrated surface POC export F_{100} (Figures 1–3; Tables 4 and 5) must be balanced on appropriate time and space scales by new production and external nutrient supply, largely from physical upwelling and mixing for most ocean regions (Ducklow & Doney, 2013). As an indicator of physical controls on export associated with nutrient supply in the individual RECCAP2 model, global-integrated F_{100} values exhibited a positive correlation with global-ocean anthropogenic CO_2 uptake (Figure 7) (DeVries et al., 2023). This is consistent with findings from previous model intercomparison exercises where models with stronger thermocline ventilation had both larger export flux and anthropogenic CO_2 uptake (Najjar et al., 2007). This correlation is due to a common underlying physical mechanism whereby stronger ventilation enhances both the downward transport of anthropogenic CO_2 and the upward transport of nutrients and thus carbon export.

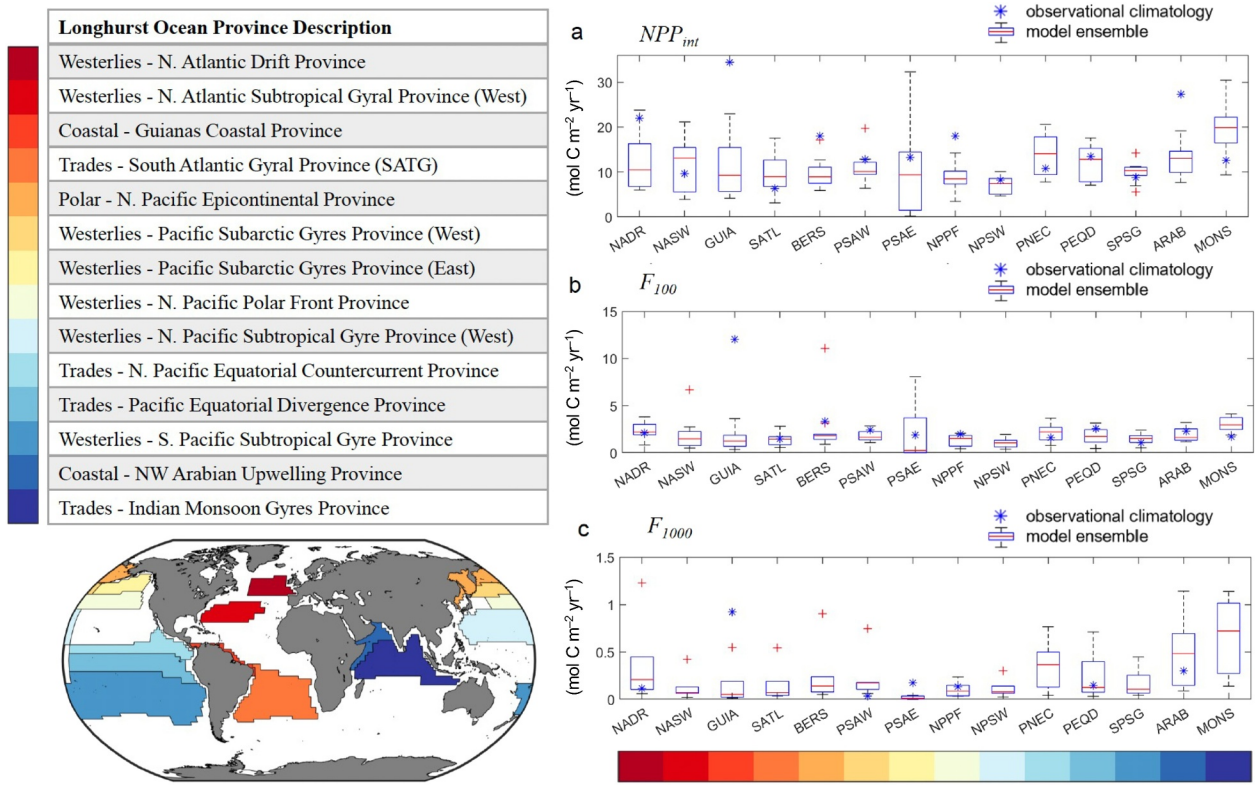

Figure 5. Biological pump metrics aggregated into Longhurst provinces (left column; Reygondeau et al., 2013) for comparison of model results with province-level observational estimates from Mouw et al. (2016b). Box-whisker plots (right column) of RECCAP2 multi-model ensemble medians, interquartile ranges, and outliers (red plus symbol when present) as well as observational estimates (blue asterisks) for annual-mean (a) vertical integrated primary production (NPP_{int}), (b) sinking particulate organic carbon (POC) fluxes at 100 m (F_{100}), and (c) sinking POC flux at 1,000 m (F_{1000}), all in mol C m^{-2} yr^{-1}, pooled into biogeochemical Longhurst ocean provinces. Robust uncertainty estimates are not available for the observational climatology, which averages available data that is often spatially sparse and/or concentrated in brief time intervals. Note that only the provinces reported in Mouw et al. (2016b) (listed in inset table and highlighted in color in map in left column) are plotted in the right column box-whisker plots.

The physical-chemical solubility mechanisms controlling ocean anthropogenic CO_2 uptake are well documented. While many Earth System model studies project substantial climate-driven changes in future ocean primary production and other biological carbon pump metrics, with potentially important climate change-biogeochemical feedbacks, contemporary observations and previous model studies (Canadell et al., 2021) as well as the RECCAP2 biogeochemical models reported here suggest relatively weak historical climate-driven trends in the biological carbon pump. As physical climate change signals continue to grow, future modeling and observational studies should continue to evaluate the capabilities to detect and attribute long-term climate-driven trends in marine biopump metrics.

Seasonal variations in upper-ocean biogeochemistry were used as a metric of the physical controls associated with seasonal mixing and nutrient supply, which are reflected in simulated POC export. By correcting for seasonal thermal variations in pCO_2 (Equation 3), we used model monthly pCO_2 fields to quantify the combined effects of seasonal biogeochemical, gas-exchange and physical processes through the seasonal amplitude of non-thermal pCO_2, $\Delta pCO_{2,\text{non-thermal}}$ (Takahashi et al., 2002). The geographic pattern of $\Delta pCO_{2,\text{non-thermal}}$ from the RECCAP2 model ensemble was similar to the pattern from the mean of the pCO_2 observational products (Figures 8a and 8b).

Both the model ensemble and observational products exhibited regional variations of $\Delta pCO_{2,\text{non-thermal}}$ that ranged from 30 to >150 µatm with elevated values in mid-to high latitudes as well as equatorial and eastern boundary current upwelling regions; relative to the pCO_2 observational products, the grid-scale $R^2 = 0.626$ with a mean model bias = −17.7 µatm. The magnitude of $\Delta pCO_{2,\text{non-thermal}}$ in the model ensemble was considerably lower than the ensemble of observational products in the mid-to high latitude northern hemisphere, eastern

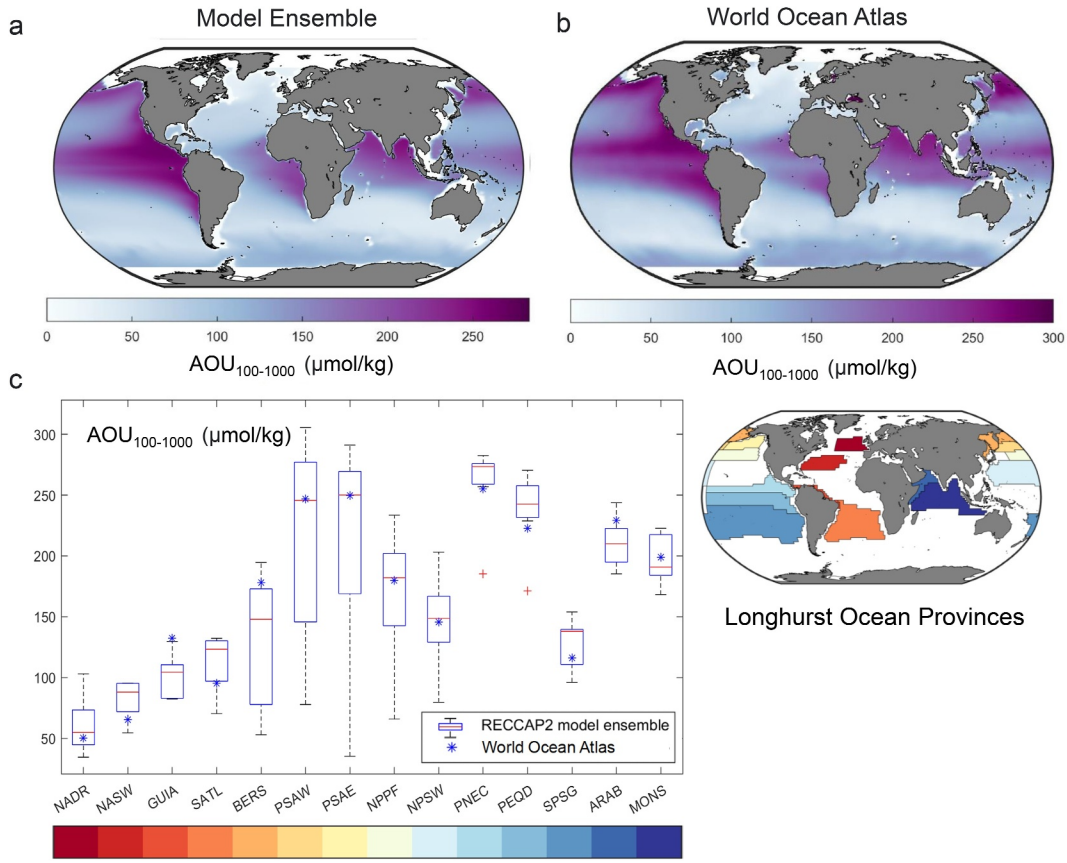

Figure 6. Analysis of apparent oxygen utilization (AOU, µmol kg^{-1}) vertically averaged over the mesopelagic zone (100–1,000 m): (a) spatial map of RECCAP2 multi-model ensemble average, and (b) spatial map from World Ocean Atlas observational data set, and (c) box-whisker plot of RECCAP2 multi-model ensemble medians, interquartile ranges, and outliers (red plus symbol when present) as well as observational estimate (blue asterisk) pooled into biogeochemical Longhurst ocean provinces (Figure 5; Reygondeau et al., 2013); note that the figure displays the same subset of provinces as in Figure 5.

tropical Pacific, and Brazil-Malvinas convergence region, suggesting a generally weaker modeled seasonal cycling of DIC. The same low bias in the RECCAP2 models was evident on the scale of Longhurst provinces where the values from many of the observational products fell at the top end or well above the model-ensemble interquartile (Figure 8c), though note the substantial disagreement across the observational products. In many ocean regions, strong seasonality in mixed layer depth modulates vertical nutrient supply and annual-mean biological productivity. The weaker model ensemble $\Delta pCO_{2,\text{non-thermal}}$ values (Figure 8), therefore, may be linked to the generally lower NPP and F_{100} values relative to observations in several polar and sub-polar provinces (Figure 5).

4. Discussion

Our analysis of the ocean biological carbon pump fields from the RECCAP2 multi-model ensemble revealed generally encouraging agreement with many aspects of observed patterns. Global-integrated NPP and surface export flux (F_{100}) from the RECCAP2 models tended to fall at the lower end of observational estimates (Figure 3 and Table 5), and geographic patterns in NPP were generally consistent with observational data products (Figures 1 and 5). Similar to previous model intercomparison studies (Laufkötter et al., 2015, 2016), we found substantial within-ensemble variation in global biological carbon pump metrics, including the presence of model outliers (Figure 3), indicating that these aspects of biogeochemical models have not necessarily converged with time.

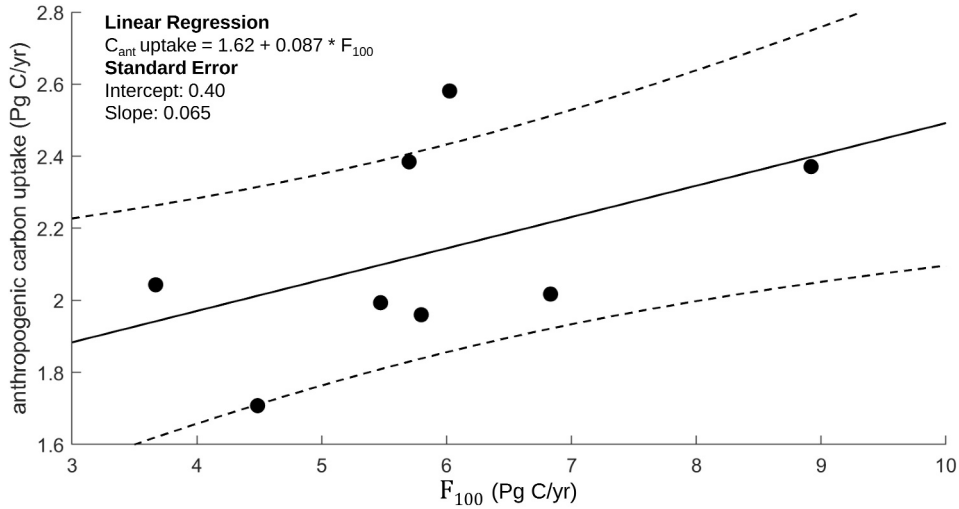

Figure 7. Scatter plot of global-integrated ocean anthropogenic CO_2 uptake (mean of 1985–2018) (Pg C yr^{-1}) versus particulate organic carbon export flux (F_{100}, Pg C yr^{-1}) for individual RECCAP2 models. Anthropogenic CO_2 uptake for the same RECCAP2 models was taken from DeVries et al. (2023). A linear regression and confidence intervals for the regression are overlain (Glover et al., 2011). The F_{100}–anthropogenic CO_2 uptake correlation was indirect through a common underlying physical mechanism whereby stronger ventilation enhances both the downward transport of anthropogenic CO_2 correlation and the upward transport of nutrients and thus F_{100}.

Regional patterns in the RECCAP2 model-mean ensemble included elevated NPP, surface export flux (F_{100}) and export efficiency (E_{100}) in high-latitudes and coastal and equatorial upwelling regions, with lower values in more oligotrophic regions. These results are in line with previous studies that found that a substantial proportion of NPP in nutrient-rich regions is driven by large phytoplankton such as diatoms and, combined with an active zooplankton population, this can generate a significant export flux in the form of both dense aggregates and fecal pellets. High-latitude elevated biomass, colder temperatures (Dunne et al., 2005), and strong seasonality have also been implicated in observations of higher POC export fluxes in spring and/or summer months contributing to the annual mean (Bol et al., 2018; Buesseler et al., 2001; Henson et al., 2023; Lampitt et al., 2001). In low nutrient regimes, such as the lower latitude oligotrophic gyres, previous studies report export flux to be low (Henson et al., 2012) but relatively constant throughout the year with small seasonal increases in fluxes (Karl et al., 2012). Future studies of the RECCAP2 ensemble could investigate in more detail the seasonality in NPP, F_{100}, and E_{100}, exploring, for example, the seasonal variability in export ratio that can be substantial due in part to the time lag between NPP and export flux (Giering et al., 2014, 2017; Henson et al., 2015; Laws & Maiti, 2019).

The sinking POC flux into the deep ocean (F_{1000}) and mesopelagic transfer efficiency across the mesopelagic zone ($E_{1000/100}$) in the RECCAP2 multi-model ensemble (Figures 1 and 5) exhibited different spatial patterns than those found for surface export, similar to findings of previous studies (e.g., Henson et al., 2012). Simulated F_{1000} and $E_{1000/100}$ were greater in the tropical eastern Pacific, eastern Atlantic, and Arabian Sea, and $E_{1000/100}$ was also elevated in the western tropical North Atlantic and, to a lesser extent, Southern Ocean. Previous model studies have also found substantial regional variations due to particle size and composition effects (Lima et al., 2014) that modify empirical power curves used for modeling POC sinking and remineralization (Martin et al., 1987). Model parameterizations tend to increase the effective remineralization length scales and thus transfer to depth in regions with high mineral fluxes (e.g., dust, $CaCO_3$, silica) (Armstrong et al., 2001) or in tropical oxygen minimum zones (Dinauer et al., 2022; Laufkötter et al., 2017). The RECCAP2 regional variations in mesopelagic transfer efficiency, modulated with basin-scale variations in physical circulation-driven sequestration time-scale (Siegel et al., 2021), influence the effect of the biological pump on ocean carbon storage (Kwon et al., 2009).

While we focused primarily on long-term mean NPP and export fluxes, the RECCAP2 models also exhibited some year-to-year variability (Table S1 in Supporting Information S1) and small long-term temporal trends (Table S2 in Supporting Information S1). However, the interannual variability and trends of these metrics are quite small and typically much lower than within-ensemble model differences (Figure S2 in Supporting Information S1). No consistent positive or negative trend was observed across the models in simulated NPP and

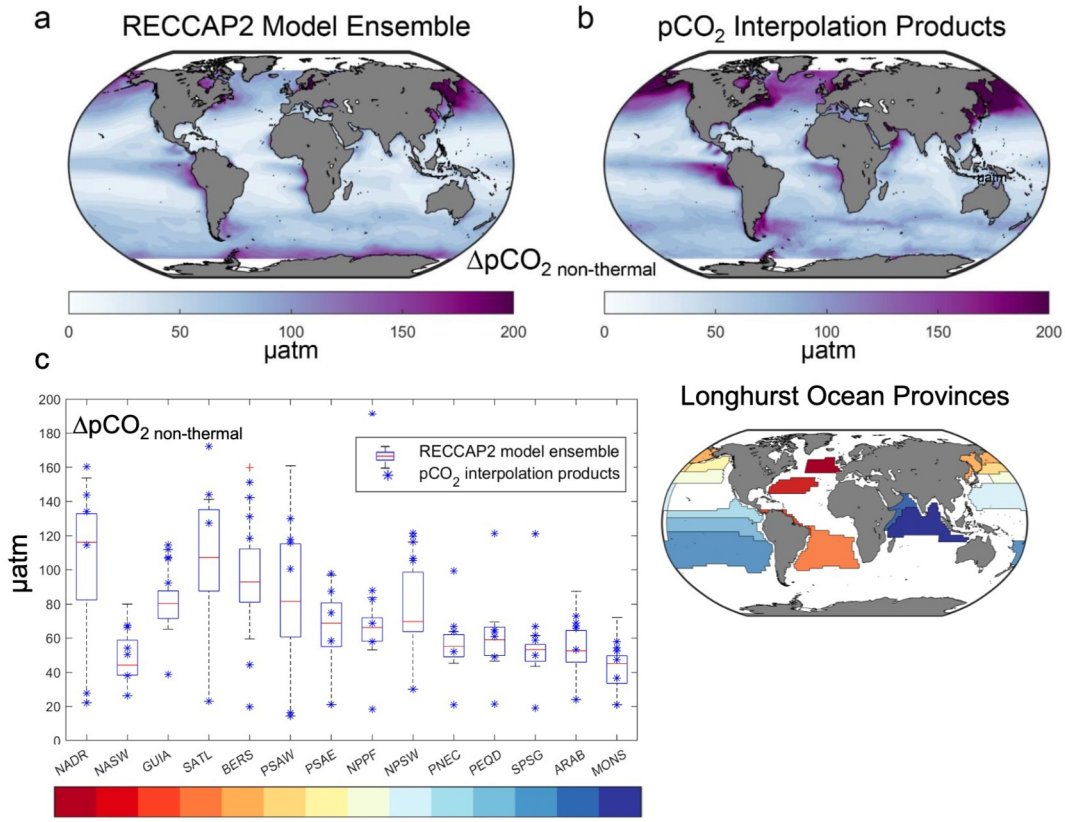

Figure 8. Analysis characterizing the combined effects of seasonal biogeochemical, gas-exchange and physical processes using the seasonal amplitude of non-thermal $\Delta pCO_{2\,non\text{-}thermal}$ (a) spatial map of RECCAP2 multi-model ensemble average, (b) spatial map from pCO_2 observational data products, and (c) box-whisker plot of RECCAP2 multi-model ensemble medians, interquartile ranges, and outliers pooled into biogeochemical Longhurst ocean provinces (Figure 5; Reygondeau et al., 2013). Note that the figure displays the same subset of provinces as in Figure 5. The province means from each observational product are plotted in panel (c) as individual points rather than as box-whiskers because of the limited number of observational products.

sinking POC fluxes at 100 and 1,000 m, with NPP trends of order ±0.01 Pg C yr^{-1}/year over the 33 years of the time series (1985–2018). Although these trends could contain a signal from climate change, this signal is not evident due to interannual variability. Previous modeling studies indicate that chlorophyll and NPP time series of 30–40 years length are needed to distinguish climate change trends from natural variability (Henson et al., 2010), though a recent study suggests that climate-change trends can emerge more rapidly in ocean color remote-sensing reflectance not reported for RECCAP2 models (Cael et al., 2023). Hence, the RECCAP2 analysis period may indeed not be long enough to separate trends from interannual variability. Furthermore, any actual climate change signal in models may be masked by temporal biases associated with incomplete model spin-up and resulting temporal drift (Séférian et al., 2016).

Our analysis of the biological carbon pump is relevant in several ways to the primary focus of the RECCAP2 ocean project on air-sea CO_2 fluxes and ocean uptake of anthropogenic CO_2 (DeVries et al., 2023). Biological net CO_2 uptake and carbon export modulate the pre-industrial and contemporary spatial and seasonal patterns of surface ocean pCO_2 and sea-air CO_2 flux that must be accounted for to determine anthropogenic CO_2 perturbations. The low model F_{100} values globally (Figure 3) and for mid-to high-latitude Northern Hemisphere and eastern equatorial Pacific provinces (Figure 5), relative to observations, suggested that the RECCAP2 model ensemble may have underestimated biological CO_2 drawdown in high productivity regions. A weak regional biological pump (Figure 5) could also contribute to the weaker $\Delta pCO_{2,non\text{-}thermal}$ values found at mid-to high-latitudes and in the eastern equatorial Pacific in the model ensemble relative to observations (Figure 8). Future work with more detailed model diagnostics could explore the connections between regional biases in simulated

annual-mean and seasonal export production and biases in air-sea CO_2 flux as observed in other RECCAP2 studies (DeVries et al., 2023; Hauck et al., 2023).

Ocean circulation modulates biological export flux on basin to global scales (Najjar et al., 2007), and the range in RECCAP2 global-integrated F_{100} values indicated that substantial differences exist in simulated ocean physics within the RECCAP2 marine biogeochemical models (Doney et al., 2004). The same ocean circulation variations also likely influenced the anthropogenic CO_2 uptake estimates from DeVries et al. (2023), as indicated by the positive correlation between anthropogenic CO_2 uptake and F_{100} across individual RECCAP2 models (Figure 7). This is supported by further analysis of the RECCAP2 models demonstrating that the rate of ocean overturning circulation is strongly correlated with anthropogenic CO_2 uptake in the models (Terhaar et al., 2024). Variations in model export could also be compared against metrics of physical stratification (Fu et al., 2022) and subsurface oxygen fields that integrate both biological respiration and physical ventilation (Takano et al., 2023). The substantial inter-model spread in both physical and biogeochemical metrics likely reflects common factors resulting from differences in simulated thermocline ventilation and exchange between the surface and mid-depth ocean. There may also be utility in comparing ocean physical-biogeochemical model results from historical and contemporary periods from forced ocean-only hindcast simulations and full coupled climate simulations using standardized protocols such as those from the Ocean Model Intercomparison Project (OMIP) (Griffies et al., 2016; Orr et al., 2017).

A set of additional model development recommendations emerged from our analyses. One path forward would leverage independent model skill evaluation for inert chemical tracers (e.g., CFC-11, CFC-12, SF_6) using standard ocean model intercomparison protocols (e.g., CMIP6 OMIP; Orr et al., 2017). The transient tracer simulations would help decipher the physical-biological factors controlling the simulated AOU (Figure 6). Remineralization of sinking biological organic matter structures sub-surface ocean DIC, O_2, and nutrient fields, a signal that must be addressed in observational estimates of anthropogenic CO_2. While the predominant pathway for ocean anthropogenic CO_2 uptake involves physical-chemical dynamics, rather than biological dynamics, the same physical circulation and mixing processes influence biogeochemical rates such as nutrient supply. Therefore, evaluation and improvement of the simulated ocean biological pump may also improve the model representation of anthropogenic carbon uptake.

The substantial variation in biological pump metrics shown here highlights the need to reconcile inter-model and model-observational differences. Challenges arise for model improvement because there is limited agreement on the appropriate parameterizations for many key processes of biological carbon export (Henson et al., 2022), subsurface particle sinking, and remineralization. Many global models include detailed representation of euphotic zone processes but rather a more simplistic representation of mesopelagic processes. Thus, the simulated global-scale biological carbon pump responses to interannual variability, let alone decadal climate change, remain poorly constrained (Henson et al., 2016). Following the mechanistic approach reported in previous model intercomparison studies for primary production (Laufkötter et al., 2015) and export production (Laufkötter et al., 2016), future studies could emphasize how overall model behavior reflects differences in model parameterizations, functional equations, and parameter values in both the euphotic and mesopelagic zones. The hyperspectral capabilities from NASA's recently launched Plankton, Aerosol, Clouds, ocean Ecosystem (PACE) mission also offer new opportunities for evaluating simulated phytoplankton community composition fields and developing new model parameterizations (Cetinić et al., 2024).

Opportunities exist to leverage process-level information from lab and field studies to improve model treatment of POC production, sinking POC flux and extension of export pathways beyond POC gravitational sinking, for example, physical subduction and active migration by organisms (Boyd et al., 2019; Henson et al., 2022; Siegel et al., 2016, 2023). Phytoplankton community structure, captured to some degree in many models (Table 2), influences the magnitude and composition of export flux from the euphotic zone, the heterotrophic consumers of sinking POC and zooplankton community structure (Boyd & Newton, 1995; Cavan et al., 2019). Model treatments could be improved for grazers such as zooplankton that decrease particle flux by consuming phytoplankton and sinking POC, while also increasing flux by packaging POC into fecal pellets with a wide range of sinking speeds (Steinberg & Landry, 2017; Turner, 2015). Grazer diel vertical migration may also need to be incorporated as a carbon shunt below the depth horizons of most intense heterotrophic activity (i.e., upper mesopelagic zone), consuming POC in the surface ocean and respiring it at grazer resident daytime depth (Bianchi et al., 2013).

More mechanistic treatment of particle dynamics may also be feasible. Particle disaggregation, physically through shear or biologically through fragmentation by grazers, likely contributes substantially to the decline in POC flux with depth while also providing a POC source for mesopelagic microbes (Briggs et al., 2020; Laurenceau-Cornec et al., 2020). Microbes can also directly reduce POC flux, as they constantly attach and detach from sinking POC (Kiørboe et al., 2002, 2003), hydrolyzing and respiring the POC. While variable particle sinking speed is included in some model parameterizations, large meta-analyses of empirical data have struggled to find a strong link between sinking rate and size of particles because of the vast variability in particle type, methods used to measure sinking rate, and environment from which the particles were collected (Cael et al., 2021).

5. Conclusions

The analysis of the RECCAP2 ocean biogeochemical model ensemble identified generally encouraging model-data agreement in large-scale spatial patterns of particulate organic carbon production and sinking flux, though with substantial spread in biopump metrics across the model ensemble and observational products. Model ensemble export flux at 100 m F_{100} and export ratio F_{100}/NPP fell at the lower end of observational estimates, and there is some indication that the model ensemble may have underestimated regional biological CO_2 drawdown and air-sea CO_2 flux in high productivity regions. Recognizing the more limited observational constraints, the analysis found approximate model-data agreement for the particulate organic carbon flux at 1,000 m F_{1000} and mesopelagic transfer efficiency F_{1000}/F_{100}. Substantial model-data biases were identified for all the biological carbon pump metrics in some ocean regions.

The RECCAP2 analysis presented standard ocean biological carbon pump metrics for accessing biogeochemical model skill, and the identified model biases should be used to guide directions for future model development. Many of new process-level insights from ocean field and remote sensing studies (Osborne et al., 2023) are already driving progress on improved mechanistic parameterizations for sinking particle flux (e.g., Dinauer et al., 2022), vertical migration (e.g., Archibald et al., 2019), and other key factors in the marine biological pump. Together with global-scale ocean biogeochemical data compilations and syntheses (e.g., Clements et al., 2023; Mouw et al., 2016a; Mouw et al., 2016b), there are now promising new opportunities to evaluate, constrain, and improve ocean biological carbon pump simulations.

Despite decades of research on GOBMs, the RECCAP2 analysis demonstrated that there remain large spreads in the simulated biological pump metrics across the suite of RECCAP2 models. For example, the within-ensemble standard deviation for export flux at the base of the euphotic zone F_{100} is of the order of 20% of the ensemble mean, and the fractional standard deviation is even larger at about 35% for POC flux at 1,000 m F_{1000}. Even acknowledging limitations in observational constraints, the large spread in these key simulated carbon cycle metrics suggests that there is no simple resolution by adjusting a single parameterization or parameter value. Nutrient supply to the upper ocean, biological export, remineralization profiles, and nutrient fields involve coupled and complex biophysical dynamics, and resolution of remaining ocean biological pump uncertainties will likely involve careful and thoughtful analysis of system-level interactions between ocean physics and biogeochemistry. In future studies, we recommend that biogeochemical models should be further refined to better represent physical and biological processes affecting carbon export, and that increasing the number and quality of carbon export observations is critical for improving our understanding of the ocean's biological carbon pump.

Acknowledgments
S.C. Doney and K.A. Mitchell acknowledge support from the U.S. National Science Foundation via the Center for Chemical Currencies of a Microbial Planet (C-CoMP, NSF 2019589), and this is C-CoMP publication number 038. S.A. Henson received support from a European Research Council Consolidator Grant (GOCART, agreement number 724416). S. Henson and J. Hauck received support from the European Union's Horizon 2020 research and innovation program under Grant agreement no. 820989 (COMFORT), and the European Union's Horizon Europe research and innovation programme under Grant agreement no. 101083922 (OceanICU). Funding to J. Hauck was provided by the Initiative and Networking Fund of the Helmholtz Association (Helmholtz Young Investigator Group Marine Carbon and Ecosystem Feedbacks in the Earth System, MarESys, Grant VH-NG-1301). J.D. Müller and N. Gruber acknowledge support from the European Union's Horizon 2020 research and innovation programme under Grant agreement no. 821003 (project 4C) and no. 820989 (project COMFORT). T. DeVries acknowledges support from NSF Grant OCE-1958955. E.L. Cavan was funded by an Imperial College Research Fellowship.

Data Availability Statement

The RECCAP2 ocean data collection can be found in Müller (2023).

References

Archibald, K., Siegel, D. A., & Doney, S. C. (2019). Modeling the impact of zooplankton diel vertical migration on the carbon export flux of the biological pump. *Global Biogeochemical Cycles*, *33*(2), 181–199. https://doi.org/10.1029/2018GB005983

Armstrong, R. A., Lee, C., Hedges, J. I., Honjo, S., & Wakeham, S. G. (2001). A new, mechanistic model for organic carbon fluxes in the ocean based on the quantitative association of POC with ballast minerals. *Deep Sea Research Part II*, *49*(1–3), 219–236. https://doi.org/10.1016/S0967-0645(01)00101-1

Aumont, O., Ethé, C., Tagliabue, A., Bopp, L., & Gehlen, M. (2015). PISCES-v2: An ocean biogeochemical model for carbon and ecosystem studies. *Geoscientific Model Development*, *8*, 2465–2513. https://doi.org/10.5194/gmd-8-2465-2015

Bacastow, R., & Maier-Reimer, E. (1990). Ocean-circulation model of the carbon cycle. *Climate Dynamics*, *4*(2), 95–125. https://doi.org/10.1007/BF00208905

Behrenfeld, M. J., Boss, E., Siegel, D. A., & Shea, D. M. (2005). Carbon-based ocean productivity and phytoplankton physiology from space. *Global Biogeochemical Cycles*, *19*(1), GB1006. https://doi.org/10.1029/2004GB002299

Behrenfeld, M. J., & Falkowski, P. G. (1997). Photosynthetic rates derived from satellite-based chlorophyll concentration. *Limnology and Oceanography*, *42*, 1–20. https://doi.org/10.4319/lo.1997.42.1.0001

Berthet, S., Séférian, R., Bricaud, C., Chevallier, M., Voldoire, A., & Ethé, C. (2019). Evaluation of an online grid-coarsening algorithm in a global eddy-admitting ocean-biogeochemical model. *Journal of Advances in Modeling Earth Systems*, *11*(6), 1759–1783. https://doi.org/10.1029/2019ms001644

Bianchi, D., Stock, C., Galbraith, E. D., & Sarmiento, J. L. (2013). Diel vertical migration: Ecological controls and impacts on the biological pump in a one-dimensional ocean model. *Global Biogeochemical Cycles*, *27*(2), 478–491. https://doi.org/10.1002/gbc.20031

Bol, R., Henson, S. A., Rumyantseva, A., & Briggs, N. (2018). High-frequency variability of small-particle carbon export flux in the Northeast Atlantic. *Global Biogeochemical Cycles*, *32*(12), 1803–1814. https://doi.org/10.1029/2018GB005963

Boyd, P., & Newton, P. (1995). Evidence of the potential influence of planktonic community structure on the interannual variability of particulate organic carbon flux. *Deep Sea Research Part I*, *42*(5), 619–639. https://doi.org/10.1016/0967-0637(95)00017-Z

Boyd, P. W., Claustre, H., Levy, M., Siegel, D. A., & Weber, T. (2019). Multi-faceted particle pumps drive carbon sequestration in the ocean. *Nature*, *568*(7752), 327–335. https://doi.org/10.1038/s41586-019-1098-2

Briggs, N., Dall'Olmo, G., & Claustre, H. (2020). Major role of particle fragmentation in regulating biological sequestration of CO_2 by the oceans. *Science*, *367*(6479), 791–793. https://doi.org/10.1126/science.aay1790

Broecker, W. S., & Peng, T. H. (1982). *Tracers in the sea* (p. 690). Eldigio Press. Retrieved from https://www.ldeo.columbia.edu/~broecker/Home_files/TracersInTheSea_searchable.pdf

Buesseler, K. O., Ball, K. O. L., Andrews, J., Cochran, J. K., Hirschberg, D. J., Bacon, M. P., et al. (2001). Upper ocean export of particulate organic carbon and biogenic silica in the Southern Ocean along 170°W. *Deep Sea Research Part II*, *48*(19–20), 4275–4297. https://doi.org/10.1016/S0967-0645(01)00089-3

Burd, A. B. (2024). Modeling the vertical flux of organic carbon in the global ocean. *Annual Review of Marine Science*, *16*(1), 135–161. https://doi.org/10.1146/annurev-marine-022123-102516

Cael, B. B., Bisson, K., Boss, E., Dutkiewicz, S., & Henson, S. (2023). Global climate-change trends detected in indicators of ocean ecology. *Nature*, *619*(7970), 551–554. https://doi.org/10.1038/s41586-023-06321-z

Cael, B. B., Cavan, E. L., & Britten, G. L. (2021). Reconciling the size-dependence of marine particle sinking speed. *Geophysical Research Letters*, *48*(5), e2020GL091771. https://doi.org/10.1029/2020GL091771

Canadell, J. G., Monteiro, P. M. S., Costa, M. H., Cotrim da Cunha, L., Cox, P. M., Eliseev, A. V., et al. (2021). Global carbon and other biogeochemical cycles and feedbacks. In V. Masson-Delmotte, P. Zhai, A. Pirani, S. L. Connors, C. Péan, S. Berger, et al. (Eds.), *Climate Change 2021: The Physical Science Basis. Contribution of Working Group I to the Sixth Assessment Report of the Intergovernmental Panel on Climate Change* (pp. 673–816). Cambridge University Press. https://doi.org/10.1017/9781009157896.007

Carr, M., Friedrichs, M., Schmeltz, M., Noguchiaita, M., Antoine, D., Arrigo, K., et al. (2006). A comparison of global estimates of marine primary production from ocean color. *Deep-Sea Research Part II*, *53*(5–7), 741–770. https://doi.org/10.1016/j.dsr2.2006.01.028

Carr, M. E. (2002). Estimation of potential productivity in Eastern Boundary Currents using remote sensing. *Deep Sea Research Part II*, *49*(1–3), 59–80. https://doi.org/10.1029/2021GB007162

Carroll, D., Menemenlis, D., Adkins, J. F., Bowman, K. W., Brix, H., Dutkiewicz, S., et al. (2020). The ECCO-Darwin data-assimilative global ocean biogeochemistry model: Estimates of seasonal to multidecadal surface ocean pCO_2 and air-sea CO_2 flux. *Journal of Advances in Modeling Earth Systems*, *12*(10), e2019MS001888. https://doi.org/10.1029/2019MS001888

Carroll, D., Menemenlis, D., Dutkiewicz, S., Lauderdale, J. M., Adkins, J. F., Bowman, K. W., et al. (2022). Attribution of space-time variability in global-ocean dissolved inorganic carbon. *Global Biogeochemical Cycles*, *36*(3), e2021GB007162. https://doi.org/10.1029/2021GB007162

Cavan, E. L., Laurenceau-Cornec, E. C., Bressac, M., & Boyd, P. W. (2019). Exploring the ecology of the mesopelagic biological pump. *Progress in Oceanography*, *176*, 102125. https://doi.org/10.1016/j.pocean.2019.102125

Cetinić, I., Rousseaux, C. S., Carroll, I. T., Chase, A. P., Kramer, S. J., Werdell, P. J., et al. (2024). Phytoplankton composition from sPACE: Requirements, opportunities, and challenges. *Remote Sensing of Environment*, *302*, 113964. https://doi.org/10.1016/j.rse.2023.113964

Chau, T. T. T., Gehlen, M., & Chevallier, F. (2022). A seamless ensemble-based reconstruction of surface ocean pCO_2 and air–sea CO_2 fluxes over the global coastal and open oceans. *Biogeosciences*, *19*(4), 1087–1109. https://doi.org/10.5194/bg-19-1087-2022

Clements, D. J., Yang, S., Weber, T., McDonnell, A. M. P., Kiko, R., Stemmann, L., & Bianchi, D. (2023). New estimate of organic carbon export from optical measurements reveals the role of particle size distribution and export horizon. *Global Biogeochemical Cycles*, *37*(3), e2022GB007633. https://doi.org/10.1029/2022GB007633

Cram, J. A., Weber, T., Leung, S. W., McDonnell, A. M. P., Liang, J.-H., & Deutsch, C. (2018). The role of particle size, ballast, temperature, and oxygen in the sinking flux to the deep sea. *Global Biogeochemical Cycles*, *32*(5), 858–876. https://doi.org/10.1029/2017GB005710

Crisp, D., Dolman, H., Tanhua, T., McKinley, G. A., Hauck, J., Bastos, A., et al. (2022). How well do we understand the land-ocean-atmosphere carbon cycle? *Reviews of Geophysics*, *60*(2), e2021RG000736. https://doi.org/10.1029/2021RG000736

DeVries, T. (2022). The ocean carbon cycle. *Annual Review of Environment and Resources*, *47*(1), 317–341. https://doi.org/10.1146/annurev-environ-120920-111307

DeVries, T., Le Quéré, C., Andrews, O., Berthet, S., Hauck, J., Ilyina, T., et al. (2019). Decadal trends in the ocean carbon sink. *Proceedings of the National Academy of Sciences*, *116*(24), 11646–11651. https://doi.org/10.1073/pnas.1900371116

DeVries, T., & Weber, T. (2017). The export and fate of organic matter in the ocean: New constraints from combining satellite and oceanographic tracer observations. *Global Biogeochemical Cycles*, *31*(3), 535–555. https://doi.org/10.1002/2016GB005551

DeVries, T., Yamamoto, K., Wanninkhof, R., Gruber, N., Hauck, J., Müller, J. D., et al. (2023). Magnitude, trends, and variability of the global ocean carbon sink from 1985-2018. *Global Biogeochemical Cycles*, *37*(10), e2023GB007780. https://doi.org/10.1029/2023GB007780

Dinauer, A., Laufkötter, C., Doney, S. C., & Joos, F. (2022). What controls the large-scale efficiency of carbon transfer through the ocean's mesopelagic zone? Insights from a new, mechanistic model (MSPACMAM). *Global Biogeochemical Cycles*, *36*(10), e2021GB007131. https://doi.org/10.1029/2021GB007131

Doney, S. C., Lima, I., Feely, R. A., Glover, D. M., Lindsay, K., Mahowald, N., et al. (2009). Mechanisms governing interannual variability in upper-ocean inorganic carbon system and air–sea CO_2 fluxes: Physical climate and atmospheric dust. *Deep Sea Research Part II: Topical Studies in Oceanography*, *56*(8–10), 640–655. https://doi.org/10.1016/j.dsr2.2008.12.006

Doney, S. C., Lindsay, K., Caldeira, K., Campin, J.-M., Drange, H., Dutay, J. C., et al. (2004). Evaluating global ocean carbon models: The importance of realistic physics. *Global Biogeochemical Cycles*, *18*(3), GB3017. https://doi.org/10.1029/2003GB002150

Doney, S. C., Lindsay, K., Fung, I., & J. John, J. (2006). Natural variability in a stable 1000 year coupled climate-carbon cycle simulation. *Journal of Climate*, *19*(13), 3033–3054. https://doi.org/10.1175/JCLI3783.1

Doney, S. C., Yeager, S., Danabasoglu, G., Large, W. G., & McWilliams, J. C. (2007). Mechanisms governing interannual variability of upper ocean temperature in a global hindcast simulation. *Journal of Physical Oceanography*, *37*(7), 1918–1938. https://doi.org/10.1175/JPO3089.1

Döscher, R., Acosta, M., Alessandri, A., Anthoni, P., Arsouze, T., Bergman, T., et al. (2022). The EC-Earth3 Earth system model for the Coupled Model Intercomparison Project 6. *Geoscientific Model Development*, *15*(7), 2973–3020. https://doi.org/10.5194/gmd-15-2973-2022

Ducklow, H. W., & Doney, S. C. (2013). What is the metabolic state of the oligotrophic ocean? A debate. *Annual Review of Marine Science*, *5*(1), 525–533. https://doi.org/10.1146/annurev-marine-121211-172331

Dunne, J. P., Armstrong, R. A., Gnanadesikan, A., & Sarmiento, J. L. (2005). Empirical and mechanistic models for the particle export ratio. *Global Biogeochemical Cycles*, *19*(4), GB4026. https://doi.org/10.1029/2004GB002390

Dunne, J. P., Sarmiento, J. L., & Gnanadesikan, A. (2007). A synthesis of global particle export from the surface ocean and cycling through the ocean interior and on the seafloor. *Global Biogeochemical Cycles*, *21*(4), GB4006. https://doi.org/10.1029/2006GB002907

Dutay, J.-C., Bullister, J. L., Doney, S. C., Orr, J. C., Najjar, R., Caldeira, K., et al. (2002). Evaluation of ocean model ventilation with CFC-11: Comparison of 13 global ocean models. *Ocean Modelling*, *4*(2), 89–120. https://doi.org/10.1016/S1463-5003(01)00013-0

Falkowski, P. G., Barber, R. T., & Smetacek, V. (1998). Biogeochemical controls and feedbacks on ocean primary production. *Science*, *281*(5374), 200–206. https://doi.org/10.1126/science.281.5374.200

Fay, A. R., & McKinley, G. A. (2014). Global open-ocean biomes: Mean and temporal variability. *Earth System Science Data*, *6*(2), 273–284. https://doi.org/10.5194/essd-6-273-2014

Fennel, K., Mattern, J. P., Doney, S. C., Bopp, L., Moore, A. M., Wang, B., & Yu, L. (2022). Ocean biogeochemical modelling. *Nature Reviews Methods Primers*, *2*(1), 76. https://doi.org/10.1038/s43586-022-00154-2

Friedlingstein, P., O'Sullivan, M., Jones, M. W., Andrew, R. M., Gregor, L., Hauck, J., et al. (2022). Global carbon budget 2022. *Earth System Science Data*, *14*(11), 4811–4900. https://doi.org/10.5194/essd-14-4811-2022

Fu, W., Moore, J. K., Primeau, F., Collier, N., Ogunro, O. O., Hoffman, F. M., & Randerson, J. T. (2022). Evaluation of ocean biogeochemistry and carbon cycling in CMIP earth system models with the International Ocean Model Benchmarking (IOMB) software system. *Journal of Geophysical Research: Oceans*, *127*(10), e2022JC018965. https://doi.org/10.1029/2022JC018965

Garcia, H. E., Weathers, K., Paver, C. R., Smolyar, I., Boyer, T. P., Locarnini, R. A., et al. (2019). World Ocean Atlas 2018, Volume 3: Dissolved oxygen, apparent oxygen utilization, and oxygen saturation. In A. Mishonov (Ed.), *NOAA Atlas NESDIS* (Vol. 83, p. 38). Retrieved from https://www.ncei.noaa.gov/sites/default/files/2020-04/woa18_vol3.pdf

Giering, S., Sanders, R., Lampitt, R., Anderson, T. R., Tamburini, C., Boutrif, M., et al. (2014). Reconciliation of the carbon budget in the ocean's twilight zone. *Nature*, *507*(7493), 480–483. https://doi.org/10.1038/nature13123

Giering, S. L. C., Sanders, R., Martin, A. P., Henson, S. A., Riley, J. S., Marsay, C. M., & Johns, D. G. (2017). Particle flux in the oceans: Challenging the steady state assumption. *Global Biogeochemical Cycles*, *31*(1), 159–171. https://doi.org/10.1002/2016GB005424

Gloege, L., Yan, M., Zheng, T., & McKinley, G. A. (2022). Improved quantification of ocean carbon uptake by using machine learning to merge global models and pCO_2 data. *Journal of Advances in Modeling Earth Systems*, *14*(2), e2021MS002620. https://doi.org/10.1029/2021ms002620

Glover, D. M., Jenkins, W. J., & Doney, S. C. (2011). *Modeling methods for marine science*. Cambridge University Press. https://doi.org/10.1017/CBO9780511975721

Gregor, L., & Gruber, N. (2021). OceanSODA-ETHZ: A global gridded data set of the surface ocean carbonate system for seasonal to decadal studies of ocean acidification. *Earth System Science Data*, *13*(2), 777–808. https://doi.org/10.5194/essd-13-777-2021

Griffies, S. M., Danabasoglu, G., Durack, P. J., Adcroft, A. J., Balaji, V., Böning, C. W., et al. (2016). OMIP contribution to CMIP6: Experimental and diagnostic protocol for the physical component of the Ocean Model Intercomparison Project. *Geoscientific Model Development*, *9*, 3231–3296. https://doi.org/10.5194/gmd-9-3231-2016

Gruber, N., Bakker, D. C. E., DeVries, T., Gregor, L., Hauck, J., Landschützer, P., et al. (2023). Trends and variability in the ocean carbon sink. *Nature Reviews Earth and Environment*, *4*(2), 119–134. https://doi.org/10.1038/s43017-022-00381-x

Guidi, L., Legendre, L., Reygondeau, G., Uitz, J., Stemmann, L., & Henson, S. A. (2015). A new look at ocean carbon remineralization for estimating deep water sequestration. *Global Biogeochemical Cycles*, *29*(7), 1044–1059. https://doi.org/10.1002/2014GB005063

Hauck, J., Gregor, L., Nissen, C., Patara, L., Hague, M., Mongwe, P., et al. (2023). The Southern Ocean carbon cycle 1985–2018: Mean, seasonal cycle, trends, and storage. *Global Biogeochemical Cycles*, *37*(11), e2023GB007848. https://doi.org/10.1029/2023GB007848

Hauck, J., Völker, C., Wang, T., Hoppema, M., Losch, M., & Wolf-Gladrow, D. A. (2013). Seasonally different carbon flux changes in the Southern Ocean in response to the southern annular mode. *Global Biogeochemical Cycles*, *27*(4), 1236–1245. https://doi.org/10.1002/2013GB004600

Hauck, J., Zeising, M., Le Quéré, C., Gruber, N., Bakker, D. C. E., Bopp, L., et al. (2020). Consistency and challenges in the ocean carbon sink estimate for the global carbon budget. *Frontiers in Marine Science*, *7*, 571720. https://doi.org/10.3389/fmars.2020.571720

Henson, S. A., Beaulieu, C., & Lampitt, R. (2016). Observing climate change trends in ocean biogeochemistry: When and where. *Global Change Biology*, *22*(4), 1561–1571. https://doi.org/10.1111/gcb.13152

Henson, S. A., Briggs, N., Carvalho, F., Manno, C., Mignot, A., & Thomalla, S. (2023). A seasonal transition in biological carbon pump efficiency in the northern Scotia Sea, Southern Ocean. *Deep Sea Research Part II*, *208*, 105274. https://doi.org/10.1016/j.dsr2.2023.105274

Henson, S. A., Kelsey Bisson, K., Hammond, M. L., Martin, A., Mouw, C., & Yool, A. (2024). Effect of sampling bias on global estimates of ocean carbon export. *Environmental Research Letters*, *19*(2), 024009. https://doi.org/10.1088/1748-9326/ad1e7f

Henson, S. A., Laufkötter, C., Leung, S., Giering, S. L. C., Palevsky, H. I., & Cavan, E. L. (2022). Uncertain response of ocean biological carbon export in a changing world. *Nature Geoscience*, *15*(4), 248–254. https://doi.org/10.1038/s41561-022-00927-0

Henson, S. A., Sanders, R., & Madsen, E. (2012). Global patterns in efficiency of particulate organic carbon export and transfer to the deep ocean. *Global Biogeochemical Cycles*, *26*(1), GB1028. https://doi.org/10.1029/2011GB004099

Henson, S. A., Sarmiento, J. L., Dunne, J. P., Bopp, L., Lima, I., Doney, S. C., et al. (2010). Detection of anthropogenic climate change in satellite records of ocean chlorophyll and productivity. *Biogeosciences*, *7*(2), 621–640. https://doi.org/10.5194/bg-7-621-2010

Henson, S. A., Yool, A., & Sanders, R. (2015). Variability in efficiency of particulate organic carbon export: A model study. *Global Biogeochemical Cycles*, *29*(1), 33–45. https://doi.org/10.1002/2014GB004965

Hood, R. R., Laws, E. A., Armstrong, R. A., Bates, N. R., Brown, C. W., Carlson, C. A., et al. (2006). Pelagic functional group modeling: Progress, challenges and prospects. *Deep-Sea Research II*, *53*(5–7), 459–512. https://doi.org/10.1016/j.dsr2.2006.01.025

Ilyina, T., Six, K. D., Segschneider, J., Maier-Reimer, E., Li, H., & Núñez-Riboni, I. (2013). Global ocean biogeochemistry model HAMOCC: Model architecture and performance as component of the MPI-Earth system model in different CMIP5 experimental realizations. *Journal of Advances in Modeling Earth Systems*, *5*(2), 287–315. https://doi.org/10.1029/2012ms000178

Iversen, M. H. (2023). Carbon export in the ocean: A biologist's perspective. *Annual Review of Marine Science*, *15*(1), 357–381. https://doi.org/10.1146/annurev-marine-032122-035153

Karl, D. M., Church, M. J., Dore, J. E., Letelier, R., & Mahaffey, C. (2012). Predictable and efficient carbon sequestration in the North Pacific Ocean supported by symbiotic nitrogen fixation. *Proceedings of the National Academy of Sciences USA*, *109*(6), 1842–1849. https://doi.org/10.1073/pnas.1120312109

Khatiwala, S., Tanhua, T., Mikaloff Fletcher, S., Gerber, M., Doney, S. C., Graven, H. D., et al. (2013). Global ocean storage of anthropogenic carbon. *Biogeosciences*, *10*(4), 2169–2191. https://doi.org/10.5194/bg-10-2169-2013

Kiørboe, T., Grossart, H.-P., Ploug, H., & Tang, K. (2002). Mechanisms and rates of bacterial colonization of sinking aggregates. *Applied and Environmental Microbiology*, *68*(8), 3996–4006. https://doi.org/10.1128/AEM.68.8.3996-4006.2002

Kiørboe, T., Tang, K., Grossart, H.-P., & Ploug, H. (2003). Dynamics of microbial communities on marine snow aggregates: Colonization, growth, detachment, and grazing mortality of attached bacteria. *Applied and Environmental Microbiology*, *69*(6), 3036–3047. https://doi.org/10.1128/AEM.69.6.3036-3047.2003

Kwon, E., Primeau, F., & Sarmiento, J. (2009). The impact of remineralization depth on the air–sea carbon balance. *Nature Geoscience*, *2*(9), 630–635. https://doi.org/10.1038/ngeo612

Lam, P. J., Doney, S. C., & Bishop, J. K. B. (2011). The dynamic ocean biological pump: Insights from a global compilation of particulate organic carbon, $CaCO_3$, and opal concentration profiles from the mesopelagic. *Global Biogeochemical Cycles*, *25*(3), GB3009. https://doi.org/10.1029/2010GB003868

Lampitt, R. S., Bett, B. J., Kiriakoulakis, K., Popova, E. E., Ragueneau, O., Vangriesheim, A., & Wolff, G. A. (2001). Material supply to the abyssal seafloor in the Northeast Atlantic. *Progress in Oceanography*, *50*(1–4), 27–63. https://doi.org/10.1016/S0079-6611(01)00047-7

Landschützer, P., Gruber, N., & Bakker, D. C. E. (2016). Decadal variations and trends of the global ocean carbon sink. *Global Biogeochemical Cycles*, *30*(10), 1396–1417. https://doi.org/10.1002/2015gb005359

Landschützer, P., Gruber, N., Bakker, D. C. E., Stemmler, I., & Six, K. D. (2018). Strengthening seasonal marine CO_2 variations due to increasing atmospheric CO_2. *Nature Climate Change*, *8*(2), 146–150. https://doi.org/10.1038/s41558-017-0057-x

Large, W. G., Danabasoglu, G., Doney, S. C., & McWilliams, J. C. (1997). Sensitivity to surface forcing and boundary layer mixing in a global ocean model: Annual-mean climatology. *Journal of Physical Oceanography*, *27*(11), 2418–2447. https://doi.org/10.1175/1520-0485(1997)027<2418:STSFAB>2.0.CO;2

Large, W. G., & Yeager, S. G. (2009). The global climatology of an interannually varying air–sea flux data set. *Climate Dynamics*, *33*(2–3), 341–364. https://doi.org/10.1007/s00382-008-0441-3

Laufkötter, C., John, J. G., Stock, C. A., & Dunne, J. P. (2017). Temperature and oxygen dependence of the remineralization of organic matter. *Global Biogeochemical Cycles*, *31*(7), 1038–1050. https://doi.org/10.1002/2017GB005643

Laufkötter, C., Vogt, M., Gruber, N., Aita-Noguchi, M., Aumont, O., Bopp, L., et al. (2015). Drivers and uncertainties of future global marine primary production in marine ecosystem models. *Biogeosciences*, *12*(23), 6955–6984. https://doi.org/10.5194/bg-12-6955-2015

Laufkötter, C., Vogt, M., Gruber, N., Aumont, O., Bopp, L., Doney, S. C., et al. (2016). Projected decreases in future marine export production: The role of the carbon flux through the upper ocean ecosystem. *Biogeosciences*, *13*, 4023–4047. https://doi.org/10.5194/bg-13-4023-2016

Laurenceau-Cornec, E. C., Le Moigne, F. A. C., Gallinari, M., Moriceau, B., Toullec, J., Iversen, M. I., et al. (2020). New guidelines for the application of Stokes' models to the sinking velocity of marine aggregates. *Limnology and Oceanography*, *65*(6), 1264–1285. https://doi.org/10.1002/lno.11388

Laws, E. A., D'sa, E., & Naik, P. (2011). Simple equations to estimate ratios of new or export production to total production from satellite-derived estimates of sea surface temperature and primary production. *Limnology and Oceanography: Methods*, *9*(12), 593–601. https://doi.org/10.4319/lom.2011.9.593

Laws, E. A., Falkowski, P. G., Smith Jr, W. O., Ducklow, H., & McCarthy, J. J. (2000). Temperature effects on export production in the open ocean. *Global Biogeochemical Cycles*, *14*(4), 1231–1246. https://doi.org/10.1029/1999GB001229

Laws, E. A., & Maiti, K. (2019). The relationship between primary production and export production in the ocean: Effects of time lags and temporal variability. *Deep Sea Research Part I*, *148*, 100–107. https://doi.org/10.1016/j.dsr.2019.05.006

Le Quéré, C., Buitenhuis, E. T., Moriarty, R., Alvain, S., Aumont, O., Bopp, L., et al. (2016). Role of zooplankton dynamics for Southern Ocean phytoplankton biomass and global biogeochemical cycles. *Biogeosciences*, *13*(14), 4111–4133. https://doi.org/10.5194/bg-13-4111-2016

Le Quéré, C., Harrison, S. P., Prentice, I. C., Buitenhuis, E. T., Aumont, O., Bopp, L., et al. (2005). Ecosystem dynamics based on plankton functional types for global ocean biogeochemistry models. *Global Change Biology*, *11*, 2016–2040. https://doi.org/10.1111/j.1365-2486.2005.1004.x

Liao, E., Resplandy, L., Liu, J., & Bowman, K. W. (2020). Amplification of the ocean carbon sink during El Niños: Role of poleward Ekman transport and influence on atmospheric CO_2. *Global Biogeochemical Cycles*, *34*(9), e2020GB006574. https://doi.org/10.1029/2020gb006574

Lima, I. D., Lam, P. J., & Doney, S. C. (2014). Dynamics of particulate organic carbon flux in a global ocean model. *Biogeosciences*, *11*(4), 1177–1198. https://doi.org/10.5194/bg-11-1177-2014

Lindsay, K., Bonan, G. B., Doney, S. C., Hoffman, F. M., Lawrence, D. M., Long, M. C., et al. (2014). Preindustrial-control and twentieth-century carbon cycle experiments with the Earth System Model CESM1(BGC). *Journal of Climate*, *27*(24), 8981–9005. https://doi.org/10.1175/jcli-d-12-00565.1

Lutz, M. J., Caldeira, K., Dunbar, R. B., & Behrenfeld, M. J. (2007). Seasonal rhythms of net primary production and particulate organic carbon flux to depth describe the efficiency of biological pump in the global ocean. *Journal of Geophysical Research*, *112*(C10), C10011. https://doi.org/10.1029/2006JC003706

Maier-Reimer, E. (1993). Geochemical cycles in an ocean general circulation model. Preindustrial tracer distributions. *Global Biogeochemical Cycles*, *7*(3), 645–677. https://doi.org/10.1029/93GB01355

Marra, J., Ho, C., & Trees, C. C. (2003). *An alternative algorithm for the calculation of primary production from remote sensing data*. Report LDEO 2003–1. Lamont-Doherty Earth Observatory. Retrieved from https://www.ldeo.columbia.edu/~marra/MarraAlgorithm.pdf

Marsay, C. M., Sanders, R. J., Henson, S. A., Pabortsava, K., Achterberg, E. P., & Lampitt, R. S. (2015). Attenuation of sinking particulate organic carbon flux through the mesopelagic ocean. *Proceedings of the National Academy of Sciences USA*, *112*(4), 1089–1094. https://doi.org/10.1073/pnas.1415311112

Martin, J. H., Knauer, G. A., Karl, D. M., & Broenkow, W. W. (1987). VERTEX: Carbon cycling in the northeast Pacific. *Deep-Sea Research*, *34*(2), 267–285. https://doi.org/10.1016/0198-0149(87)90086-0

Matsumoto, K., Sarmiento, J. L., Key, R. M., Bullister, J. L., Caldeira, K., Campin, J.-M., et al. (2004). Evaluation of ocean carbon cycle models with data-based metrics. *Geophysical Research Letters*, *31*(7), L07303. https://doi.org/10.1029/2003GL018970

Mauritsen, T., Bader, J., Becker, T., Behrens, J., Bittner, M., Brokopf, R., et al. (2019). Developments in the MPI-M Earth system model version 1.2 (MPI-ESM1. 2) and its response to increasing CO_2. *Journal of Advances in Modeling Earth Systems*, *11*(4), 998–1038. https://doi.org/10.1029/2018ms001400

Mikaloff Fletcher, S. E., Gruber, N., Jacobson, A. R., Gloor, M., Doney, S. C., Dutkiewicz, S., et al. (2007). Inverse estimates of the oceanic sources and sinks of natural CO_2 and their implied oceanic transport. *Global Biogeochemical Cycles*, *21*(1), GB1010. https://doi.org/10.1029/2006GB002751

Moore, J. K., Doney, S. C., & Lindsay, K. (2004). Upper ocean ecosystem dynamics and iron cycling in a global 3-D model. *Global Biogeochemical Cycles*, *18*(4), GB4028. https://doi.org/10.1029/2004GB002220

Mouw, C. B., Barnett, A., McKinley, G. A., Gloege, L., & Pilcher, D. (2016a). Global ocean particulate organic carbon flux merged with satellite parameters. *Earth System Science Data*, *8*(2), 531–541. https://doi.org/10.5194/essd-8-531-2016

Mouw, C. B., Barnett, A., McKinley, G. A., Gloege, L., & Pilcher, D. (2016b). Phytoplankton size impact on export flux in the global ocean. *Global Biogeochemical Cycles*, *30*(10), 1542–1562. https://doi.org/10.1002/2015GB005355

Müller, J. D. (2023). RECCAP2-ocean data collection [Dataset]. *Zenodo*. https://doi.org/10.5281/zenodo.7990823

Najjar, R. G., Jin, X., Louanchi, F., Aumont, O., Caldeira, K., Doney, S. C., et al. (2007). Impact of circulation on export production, dissolved organic matter and dissolved oxygen in the ocean: Results from Phase II of the Ocean Carbon-cycle Model Intercomparison Project (OCMIP-2). *Global Biogeochemical Cycles*, *21*(3), GB3007. https://doi.org/10.1029/2006GB002857

Nowicki, M., DeVries, T., & Siegel, D. A. (2022). Quantifying the carbon export and sequestration pathways of the ocean's biological carbon pump. *Global Biogeochemical Cycles*, *36*(3), e2021GB007083. https://doi.org/10.1029/2021GB007083

Omand, M. M., Govindarajan, R., He, J., & Mahadevan, A. (2020). Sinking flux of particulate organic matter in the oceans: Sensitivity to particle characteristics. *Scientific Reports*, *10*(1), 5582. https://doi.org/10.1038/s41598-020-60424-5

Orr, J. C., Najjar, R. G., Aumount, O., Bopp, L., Bullister, J. L., Danabasoglu, G., et al. (2017). Biogeochemical protocols and diagnostics for the CMIP6 Ocean Model Intercomparison Project (OMIP). *Geoscientific Model Development*, *10*(6), 2169–2199. https://doi.org/10.5194/gmd-10-2169-2017

Osborne, E., Luo, J. Y., Cetinić, I., Benway, H., & S. Menden-Deuer, S. (2023). Our evolving understanding of biological carbon export. *Eos*, *104*. https://doi.org/10.1029/2023EO230346

RECCAP2 Ocean Science Team. (2022). RECCAP2 ocean protocols. Retrieved from https://reccap2-ocean.github.io/protocols/

Reygondeau, G., Longhurst, A., Martinez, E., Beaugrand, G., Antoine, D., & Maury, O. (2013). Dynamic biogeochemical provinces in the global ocean. *Global Biogeochemical Cycles*, *27*(4), 1046–1058. https://doi.org/10.1002/gbc.20089

Rödenbeck, C., DeVries, T., Hauck, J., Le Quéré, C., & Keeling, R. F. (2022). Data-based estimates of interannual sea–air CO_2 flux variations 1957–2020 and their relation to environmental drivers. *Biogeosciences*, *19*(10), 2627–2652. https://doi.org/10.5194/bg-19-2627-2022

Rödenbeck, C., Keeling, R. F., Bakker, D. C., Metzl, N., Olsen, A., Sabine, C., & Heimann, M. (2013). Global surface-ocean pCO_2 and sea–air CO_2 flux variability from an observation-driven ocean mixed-layer scheme. *Ocean Science*, *9*(2), 193–216. https://doi.org/10.5194/os-9-193-2013

Rodgers, K. B., Schwinger, J., Fassbender, A. J., Landschützer, P., Yamaguchi, R., Frenzel, H., et al. (2023). Seasonal variability of the surface ocean carbon cycle: A synthesis. *Global Biogeochemical Cycles*, *37*(9), e2023GB007798. https://doi.org/10.1029/2023GB007798

Sailley, S., Vogt, M., Doney, S. C., Aita, M. N., Bopp, L., Buitenhuis, E. T., et al. (2013). Comparing food web structures and dynamics across a suite of global marine ecosystem models. *Ecological Modeling*, *261–262*, 43–57. https://doi.org/10.1016/j.ecolmodel.2013.04.006

Sarmiento, J. L., & Gruber, N. (2002). Anthropogenic carbon sinks. *Physics Today*, *55*(8), 30–36. https://doi.org/10.1063/1.1510279

Sarmiento, J. L., & Gruber, N. (2006). *Ocean biogeochemical dynamics*. Princeton University Press. https://doi.org/10.1017/S0016756807003755

Schlitzer, R. (2000). Applying the adjoint method for biogeochemical modeling: Export of particulate organic matter in the World Ocean. In P. Kasibhata (Ed.), *Inverse methods in biogeochemical cycles* (Vol. 114, pp. 107–124). AGU Monograph. https://doi.org/10.1029/GM114p0107

Schwinger, J., Goris, N., Tjiputra, J. F., Kriest, I., Bentsen, M., Bethke, I., et al. (2016). Evaluation of NorESM-OC (versions 1 and 1.2), the ocean carbon-cycle stand-alone configuration of the Norwegian Earth System Model (NorESM1). *Geoscientific Model Development*, *9*(8), 2589–2622. https://doi.org/10.5194/gmd-9-2589-2016

Séférian, R., Berthet, S., Yool, A., Palmiéri, J., Bopp, L., Tagliabue, A., et al. (2020). Tracking improvement in simulated marine biogeochemistry between CMIP5 and CMIP6. *Current Climate Change Reports*, *6*(3), 95–119. https://doi.org/10.1007/s40641-020-00160-0

Séférian, R., Gehlen, M., Bopp, L., Resplandy, L., Orr, J. C., Marti, O., et al. (2016). Inconsistent strategies to spin up models in CMIP5: Implications for ocean biogeochemical model performance assessment. *Geoscientific Model Development*, *9*(5), 1827–1851. https://doi.org/10.5194/gmd-9-1827-2016

Séférian, R., Nabat, P., Michou, M., Saint-Martin, D., Voldoire, A., Colin, J., et al. (2019). Evaluation of CNRM Earth-System model, CNRM-ESM2-1: Role of Earth system processes in present-day and future climate. *Journal of Advances in Modeling Earth Systems*, *11*(12), 4182–4227. https://doi.org/10.1029/2019ms001791

Siegel, D. A., Buesseler, K. O., Behrenfeld, M. J., Benitez-Nelson, C. R., Boss, E., Brzezinski, M. A., et al. (2016). Prediction of the export and fate of global ocean net primary production: The EXPORTS science plan. *Frontiers in Marine Science*, *3*, 22. https://doi.org/10.3389/fmars.2016.00022

Siegel, D. A., Buesseler, K. O., Doney, S. C., Sailley, S. F., Behrenfeld, M. J., & Boyd, P. W. (2014). Global assessment of ocean carbon export by combining satellite observations and food-web models. *Global Biogeochemical Cycles*, *28*(3), 181–196. https://doi.org/10.1002/2013gb004743

Siegel, D. A., DeVries, T., Cetinić, I., & K Bisson, K. M. (2023). Quantifying the ocean's biological pump and its carbon cycle impacts on global scales. *Annual Review of Marine Science*, *15*(1), 329–356. https://doi.org/10.1146/annurev-marine-040722-115226

Siegel, D. A., DeVries, T., Doney, S. C., & T. Bell, T. (2021). Assessing the sequestration time scales of some ocean-based carbon dioxide reduction strategies. *Environmental Research Letters*, *16*(10), 104003. https://doi.org/10.1088/1748-9326/ac0be0

Silsbe, G. M., Behrenfeld, M. J., Halsey, K. H., Milligan, A. J., & Westberry, T. K. (2016). The CAFE model: A net production model for global ocean phytoplankton. *Global Biogeochemical Cycles*, *30*(12), 1756–1777. https://doi.org/10.1002/2016GB005521

Steinberg, D. K., & Landry, M. R. (2017). Zooplankton and the ocean carbon cycle. *Annual Review of Marine Science*, *9*(1), 413–444. https://doi.org/10.1146/annurev-marine-010814-015924

Stock, C. A., Dunne, J. P., Fan, S., Ginoux, P., John, J., Krasting, J. P., et al. (2020). Ocean biogeochemistry in GFDL's Earth system model 4.1 and its response to increasing atmospheric CO_2. *Journal of Advances in Modeling Earth Systems*, *12*(10), e2019MS002043. https://doi.org/10.1029/2019ms002043

Stukel, M. R., Ohman, M. D., Kelly, T. B., & Biard, T. (2019). The roles of suspension-feeding and flux-feeding zooplankton as gatekeepers of particle flux into the mesopelagic ocean in the Northeast Pacific. *Frontiers in Marine Science*, *6*, 397. https://doi.org/10.3389/fmars.2019.00397

Takahashi, T., Olafsson, J., Goddard, J. G., Chipman, D. W., & Sutherland, S. C. (1993). Seasonal variation of CO_2 and nutrients in the high-latitude surface oceans: A comparative study. *Global Biogeochemical Cycles*, *7*(4), 843–878. https://doi.org/10.1029/93GB02263

Takahashi, T., Sutherland, S. C., Sweeney, C., Poisson, A., Metzl, N., Tilbrook, B., et al. (2002). Global sea–air CO_2 flux based on climatological surface ocean pCO_2, and seasonal biological and temperature effects. *Deep Sea Research Part II: Topical Studies in Oceanography*, *49*(9–10), 1601–1622. https://doi.org/10.1016/S0967-0645(02)00003-6

Takano, Y., Ilyina, T., Tjiputra, J., Eddebbar, Y. A., Berthet, S., Bopp, L., et al. (2023). Simulations of ocean deoxygenation in the historical era: Insights from forced and coupled models. *Frontiers in Marine Science*, *10*, 1139917. https://doi.org/10.3389/fmars.2023.1139917

Terhaar, J., Goris, N., Müller, J. D., DeVries, T., Gruber, N., Hauck, J., et al. (2024). Assessment of global ocean biogeochemistry models for ocean carbon sink estimates in RECCAP2 and recommendations for future studies. *Journal of Advances in Modeling Earth Systems*, *16*(3), e2023MS003840. https://doi.org/10.1029/2023ms003840

Tsujino, H., Nakano, H., Sakamoto, K., Urakawa, S., Hirabara, M., Ishizaki, H., & Yamanaka, G. (2017). *Reference manual for the meteorological research institute community ocean model version 4 (MRI. COMv4)* (Vol. 80, p. 306). Technical Reports of the Meteorological Research Institute.

Turner, J. T. (2015). Zooplankton fecal pellets, marine snow, phytodetritus and the ocean's biological pump. *Progress in Oceanography*, *130*, 205–248. https://doi.org/10.1016/j.pocean.2014.08.005

Urakawa, L. S., Tsujino, H., Nakano, H., Sakamoto, K., Yamanaka, G., & Toyoda, T. (2020). The sensitivity of a depth-coordinate model to diapycnal mixing induced by practical implementations of the isopycnal tracer diffusion scheme. *Ocean Modelling*, *154*, 101693. https://doi.org/10.1016/j.ocemod.2020.101693

Volk, T., & Hoffert, M. I. (1985). Ocean carbon pumps: Analysis of relative strengths and efficiencies in ocean-driven atmospheric CO_2 changes. In E. Sundquist & W. Broecker (Eds.), *The carbon cycle and atmospheric CO_2: Natural variations archean to present* (Vol. 32, pp. 99–110). American Geophysical Union (AGU). https://doi.org/10.1029/GM032P0099

Wanninkhof, R., Park, G.-H., Takahashi, T., Sweeney, C., Feely, R., Nojiri, Y., et al. (2013). Global ocean carbon uptake: Magnitude, variability and trends. *Biogeosciences*, *10*(3), 1983–2000. https://doi.org/10.5194/bg-10-1983-2013

Watson, A. J., Schuster, U., Shutler, J. D., Holding, T., Ashton, I. G., Landschützer, P., et al. (2020). Revised estimates of ocean-atmosphere CO_2 flux are consistent with ocean carbon inventory. *Nature Communications*, *11*(1), 1–6. https://doi.org/10.1038/s41467-020-18203-3

Weber, T., Cram, J. A., Leung, S. W., DeVries, T., & Deutsch, C. (2016). Deep ocean nutrients imply large latitudinal variation in particle transfer efficiency. *Proceedings of the National Academy of Sciences*, *113*(31), 8606–8611. https://doi.org/10.1073/pnas.1604414113

Wilson, J. D., Andrews, O., Katavouta, A., de Melo Viríssimo, F., Death, R. M., Adloff, M., et al. (2022). The biological carbon pump in CMIP6 models: 21st century trends and uncertainties. *Proceedings of the National Academy of Sciences USA*, *119*(29), e2204369119. https://doi.org/10.1073/pnas.2204369119

Wright, R. M., Le Quéré, C., Buitenhuis, E., Pitois, S., & Gibbons, M. J. (2021). Role of jellyfish in the plankton ecosystem revealed using a global ocean biogeochemical model. *Biogeosciences*, *18*(4), 1291–1320. https://doi.org/10.5194/bg-18-1291-2021

Yang, S., & Gruber, N. (2016). The anthropogenic perturbation of the marine nitrogen cycle by atmospheric deposition: Nitrogen cycle feedbacks and the ^{15}N Haber-Bosch effect. *Global Biogeochemical Cycles*, *30*(10), 1418–1440. https://doi.org/10.1002/2016gb005421

Zeng, J., Iida, Y., Matsunaga, T., & Shirai, T. (2022). Surface ocean CO_2 concentration and air-sea flux estimate by machine learning with modelled variable trends. *Frontiers in Marine Science*, *9*, 989233. https://doi.org/10.3389/fmars.2022.989233